

## Signal diffusion along connectome gradients and inter-hub routing differentially contribute to dynamic human brain function



Bo-yong Park<sup>a,\*</sup>, Reinder Vos de Wael<sup>a</sup>, Casey Paquola<sup>a</sup>, Sara Larivière<sup>a</sup>, Oualid Benkarim<sup>a</sup>, Jessica Royer<sup>a</sup>, Shahin Tavakol<sup>a</sup>, Raul R. Cruces<sup>a</sup>, Qiongling Li<sup>a</sup>, Sofie L. Valk<sup>b,c</sup>, Daniel S. Margulies<sup>d</sup>, Bratislav Mišić<sup>a</sup>, Danilo Bzdok<sup>a,e</sup>, Jonathan Smallwood<sup>f</sup>, Boris C. Bernhardt<sup>a,\*</sup>

<sup>a</sup> Multimodal Imaging and Connectome Analysis Lab, McConnell Brain Imaging Centre, Montreal Neurological Institute and Hospital, McGill University, Montreal, Quebec, Canada

<sup>b</sup> Institute of Neuroscience and Medicine (INM-7: Brain & Behaviour), Research Centre Jülich, Jülich, Germany

<sup>c</sup> Institute of Systems Neuroscience, Medical Faculty, Heinrich Heine University Düsseldorf, Düsseldorf, Germany

<sup>d</sup> Frontlab, Institut du Cerveau et de la Moelle épinière, UPMC UMR 1127, Inserm U 1127, CNRS UMR 7225, Paris, France

<sup>e</sup> Mila - Québec Artificial Intelligence Institute, Montreal, Quebec, Canada

<sup>f</sup> Department of Psychology, York Neuroimaging Centre, University of York, New York, United Kingdom

### ARTICLE INFO

**Keywords:**

structural connectome  
gradients  
functional dynamics  
Hidden Markov Model  
multimodal imaging  
diffusion MRI

### ABSTRACT

Human cognition is dynamic, alternating over time between externally-focused states and more abstract, often self-generated, patterns of thought. Although cognitive neuroscience has documented how networks anchor particular modes of brain function, mechanisms that describe transitions between distinct functional states remain poorly understood. Here, we examined how time-varying changes in brain function emerge within the constraints imposed by macroscale structural network organization. Studying a large cohort of healthy adults ( $n = 326$ ), we capitalized on manifold learning techniques that identify low dimensional representations of structural connectome organization and we decomposed neurophysiological activity into distinct functional states and their transition patterns using Hidden Markov Models. Structural connectome organization predicted dynamic transitions anchored in sensorimotor systems and those between sensorimotor and transmodal states. Connectome topology analyses revealed that transitions involving sensorimotor states traversed short and intermediary distances and adhered strongly to communication mechanisms of network diffusion. Conversely, transitions between transmodal states involved spatially distributed hubs and increasingly engaged long-range routing. These findings establish that the structure of the cortex is optimized to allow neural states the freedom to vary between distinct modes of processing, and so provides a key insight into the neural mechanisms that give rise to the flexibility of human cognition.

### 1. Introduction

A core assumption of neuroscience is that brain structure governs ongoing function (Batista-García-Ramó and Fernández-Verdecia, 2018; Baum et al., 2020; Becker et al., 2018; Ceric et al., 2017; Hermundstad et al., 2013; Honey et al., 2009; Mišić et al., 2016; Park and Friston, 2013; Rubinov et al., 2009; Snyder and Bauer, 2019; Suárez et al., 2020; Vázquez-Rodríguez et al., 2019; Wang et al., 2019, 2015). However, at the heart of this question is a puzzle: Brain structure remains relatively constant across time, yet the neural hardware ultimately supports the flexible manner that an organism alters its repertoire of responses in line with changing external and internal demands.

In both humans and non-human primates, links between brain structure and specific cognitive functions have been well established in a *stationary* manner (Han et al., 2009; Mišić et al., 2016; Wang et al., 2019). Although these studies highlight links between specific neural patterns and particular aspects of cognition (Honey et al., 2009; Mišić et al., 2016; Wang et al., 2015), such analyses are not well suited to understanding how the brain flexibly changes between different modes of operation (Allen et al., 2012; Bertolero et al., 2015; Friston et al., 2003; Kucyi et al., 2018; Taghia et al., 2018). At the same time, contemporary neuroscience has begun to recognize that global features of the connectome are also important in how structure gives rise to function. Such views suggest that systematic transitions across the cortex from sensorimotor regions

\* Corresponding authors.

E-mail addresses: [bo.y.park@mcgill.ca](mailto:bo.y.park@mcgill.ca) (B.-y. Park), [boris.bernhardt@mcgill.ca](mailto:boris.bernhardt@mcgill.ca) (B.C. Bernhardt).

to transmodal association areas may support increasingly abstract elements of cognition (Margulies et al., 2016; Mesulam, 1998). Moreover, although these transmodal regions are spatially distributed, they are also strongly interconnected, showing a rich-club architecture that implies a role in the control of more integrated cognitive states (Avena-Koenigsberger et al., 2019, 2018; Griffa and van den Heuvel, 2018; Mišić et al., 2016; van den Heuvel et al., 2012). In this study, we explore the hypothesis that specific features of cortical structural connectome organization support the transitions that brain makes between naturally occurring neural states.

Recent advances in techniques for measuring brain organization and function *in vivo*, such as diffusion magnetic resonance imaging (dMRI) and functional MRI (fMRI), have put systems neuroscience in an unprecedented position to understand features of brain organization that support flexible transitions between different modes of neural operation (Allen et al., 2012; Bertolero et al., 2015; Damaraju et al., 2014; Friston et al., 2003; Kucyi et al., 2018; Lee et al., 2019; Park et al., 2019, 2018b; Razi et al., 2017; Taghia et al., 2018; Vidaurre et al., 2017). Our current study combines state-of-the-art manifold learning techniques to identify compact spatial representations of cortical structural connectome organization, and we applied dynamic fMRI analysis to estimate transient functional brain states (Margulies et al., 2016; Vidaurre et al., 2017). In the structural domain, we build on work capturing topological organization of the cortex in a low dimensional manifold space, which has recently provided novel insights into human cognition at macroscale (Huntenburg et al., 2018; Margulies et al., 2016). Such techniques have been widely adopted in resting-state fMRI (rs-fMRI) studies of specific regions and the whole brain (Hong et al., 2019; Larivière et al., 2019a; Margulies et al., 2016; Vos de Wael et al., 2018). However, manifold learning applications to dMRI tractography data have so far focused on specific areas (Bajada et al., 2017; Cerliani et al., 2012), rather than addressing whole-brain connectivity. In the functional domain, we use dynamic functional connectivity analysis to capture transient features of brain function. Dynamic functional connectivity analysis has recently provided novel insights into large-scale brain organization (Allen et al., 2012; Ashourvan et al., 2017; Chai et al., 2017; Damaraju et al., 2014; Khambhati et al., 2018; Razi et al., 2017), inter-individual differences in cognitive functions (Bassett et al., 2011; Bertolero et al., 2015; Braun et al., 2015; Chai et al., 2016; Kucyi et al., 2018; Park et al., 2019; Taghia et al., 2018; Vidaurre et al., 2017), and network perturbations in prevalent brain disorders (Damaraju et al., 2014; Khambhati et al., 2015; Lee et al., 2019; Park et al., 2018a, 2018b). One method that can resolve functional dynamics is the Hidden Markov Model (HMM), a generative probabilistic framework that identifies time-varying brain states and associated connectivity profiles (Vidaurre et al., 2017). Recent studies have capitalized on HMMs to estimate the hierarchical organization of the dynamic state space in rs-fMRI data and assessed associations to cognitive phenotypes (Vidaurre et al., 2017) and task-related brain activations (Vidaurre et al., 2016). Here, HMMs were used to characterize brain states that occur at rest and to assess the correspondence between these patterns and those derived purely from structural connectomics. In particular, we examined how these changes map onto both low dimensional cortical representations of macroscale features of the cortex. We did not make a-priori predictions how structurally-defined low dimensional manifolds may relate to measures of functional dynamics, as whole-brain gradients derived from dMRI tractography data have not been systematically studied in humans nor integrated with HMM data. To however further contextualize the structure-function relationships identified in our study, we examined topological properties of structural network organization and assessed how these may implement different communication mechanisms (Avena-Koenigsberger et al., 2019, 2018; de Reus and van den Heuvel, 2013; Goñi et al., 2014; Griffa and van den Heuvel, 2018; Liang et al., 2018; Shu et al., 2018; van den Heuvel et al.,

2012; Zhao et al., 2017). These include the rich-club taxonomy, which classifies cortical organizations in terms of degree distributions into a densely interconnected rich-club core and a more locally connected periphery (Griffa and van den Heuvel, 2018; van den Heuvel et al., 2012), as well as network communication measures that can contrast more passive network diffusion mechanisms against routing strategies that preferentially follow shortest paths (Avena-Koenigsberger et al., 2019, 2018; Goñi et al., 2014).

Our study provided a low dimensional description of structural connectome architecture and explored its association to transient functional states in the resting brain. We capitalized on high-definition dMRI and rs-fMRI data provided by the Human Connectome Project (HCP) repository (Van Essen et al., 2013) and also assessed an independent locally acquired datasets with similar imaging parameters. Foresighting our results, we found evidence that cortical structural connectivity is optimized to allow for flexibility between states anchored in unimodal regions (that are well described by local properties of these regions captured by a low dimensional representations of cortical structure) and states anchored by transmodal regions (which engage in efficient long-range communication between states).

## 2. Methods

### 2.1. Participants

We assessed the minimally processed S900 release of the HCP (Van Essen et al., 2013). Participants who did not complete full imaging data and who had family relationships were excluded, resulting in a total of 326 participants (mean  $\pm$  SD age =  $28.56 \pm 3.73$  years; 55% female). Participants were randomly divided into a *Discovery* and *Replication* cohort. The *Discovery* dataset ( $n = 163$ ; age =  $28.86 \pm 3.78$  years; 60% female) was used for constructing a framework of structure-functional dynamic coupling and the *Replication* dataset ( $n = 163$ ; age =  $28.26 \pm 3.67$  years; 51% female) was used for testing reproducibility. All MRI data used in this study were publicly available and anonymized. Participant recruitment procedures and informed consent forms, including consent to share de-identified data, were previously approved by the Washington University Institutional Review Board as part of the HCP.

We replicated our findings in an independent dataset from our local site (MICA-MTL,  $n = 47$ ; age =  $30.43 \pm 6.83$  years; 35% female). This dataset was approved by the Institutional Review Board of Montreal Neurological Institute and Hospital and written and informed consent was obtained from all participants.

### 2.2. MRI acquisition

#### 2.2.1. HCP

HCP participants were scanned using a Siemens Skyra 3T at Washington University. The T1-weighted images were acquired using a magnetization-prepared rapid gradient echo (MPRAGE) sequence (repetition time (TR) = 2,400 ms; echo time (TE) = 2.14 ms; field of view (FOV) =  $224 \times 224$  mm $^2$ ; voxel size = 0.7 mm $^3$ ; and number of slices = 256). The T2-weighted structural data were obtained with the T2-SPACE sequence, with an identical geometry as the T1-weighted data but different TR (3,200 ms) and TE (565 ms). The dMRI data were acquired with the spin-echo echo-planar imaging (EPI) sequence (TR = 5,520 ms; TE = 89.5 ms; FOV =  $210 \times 180$  mm $^2$ ; voxel size = 1.25 mm $^3$ ; b-value = three different shells *i.e.*, 1,000, 2,000, and 3,000 s/mm $^2$ ; number of diffusion directions = 270; and number of b0 images = 18). The rs-fMRI data were collected using a gradient-echo EPI sequence (TR = 720 ms; TE = 33.1 ms; FOV =  $208 \times 180$  mm $^2$ ; voxel size = 2 mm $^3$ ; number of slices = 72; and number of volumes = 1,200).

During the rs-fMRI scan, participants were instructed to keep their eyes open looking at a fixation cross. Two sessions of rs-fMRI data were acquired; each of them contained data of left-to-right and right-to-left phase-encoded directions, providing up to four time series per participant.

### 2.2.2. MICA-MTL

The MICA-MTL imaging data were scanned using a Siemens Prisma 3T scanner at the Montreal Neurological Institute and Hospital. Image acquisition parameters were similar to the HCP dataset (T1-weighted: TR = 2,300 ms; TE = 3.14 ms; FOV = 256 × 180 mm<sup>2</sup>; voxel size = 0.8 mm<sup>3</sup>; and number of slices = 320; dMRI: TR = 3,500 ms; TE = 64.4 ms; FOV = 224 × 224 mm<sup>2</sup>; voxel size = 1.6 mm<sup>3</sup>; b-value = three different shells (200, 700, and 2,000 s/mm<sup>2</sup>); number of diffusion directions = 140; and number of b0 images = 3; rs-fMRI: TR = 600 ms; TE = 30 ms; FOV = 240 × 240 mm<sup>2</sup>; voxel size = 3 mm<sup>3</sup>; number of slices = 48; and number of volumes = 800).

## 2.3. Data preprocessing

### 2.3.1. HCP data

HCP data underwent the initiative's minimal preprocessing pipelines (Glasser et al., 2013). In brief, structural MRI data underwent gradient nonlinearity and b0 distortion correction, followed by co-registration between the T1-weighted and T2-weighted data using a rigid-body transformation. Bias field correction was performed by capitalizing on the inverse intensities from the T1- and T2-weighting. Processed data were nonlinearly registered to MNI152 space and the white and pial surfaces were generated by following the boundaries between different tissues (Dale et al., 1999; Fischl, 2012; Fischl et al., 1999b, 1999a). The white and pial surfaces were averaged to generate a mid-thickness surface, which was used to generate the inflated surface. The spherical surface was registered to the Conte69 template with 164k vertices (Van Essen et al., 2012) using MSMAll (Glasser et al., 2016; Robinson et al., 2014) and downsampled to a 32k vertex mesh. The dMRI data underwent b0 intensity normalization, and EPI distortions were corrected by leveraging reversed phase-encoded directions. The dMRI data was also corrected for eddy current distortions and head motion. The rs-fMRI data preprocessing involved corrections for EPI distortions and head motion, and fMRI data were registered to the T1-weighted data and subsequently to MNI152 space. Magnetic field bias correction, skull removal, and intensity normalization were performed. Noise components attributed to head movement, white matter, cardiac pulsation, arterial, and large vein related contributions were automatically removed using FIX (Salimi-Khorshidi et al., 2014). The minimal preprocessing with FIX denoising pipeline of the HCP performs a high-pass filtering with a cutoff of 2,000 s full width at half maximum (Glasser et al., 2013). Preprocessed time series were mapped to standard grayordinate space, with a cortical ribbon-constrained volume-to-surface mapping algorithm. The total mean of the time series of each left-to-right/right-to-left phase-encoded data was subtracted to adjust the discontinuity between the two datasets and they were concatenated to form a single time series data.

### 2.3.2. MICA-MTL

MICA-MTL data were processed similarly as the HCP data. In brief, T1-weighted data were deobliqued, reoriented, skull stripped, and cortical surfaces were generated using FreeSurfer (Dale et al., 1999; Fischl, 2012; Fischl et al., 1999b, 1999a). The dMRI data was processed using MRtrix (Tournier et al., 2019, 2012) including correction for susceptibility distortions, head motion, and eddy currents. The rs-fMRI data were processed using AFNI and FSL (Cox, 1996; Jenkinson et al., 2012). The first five volumes were discarded to allow for magnetic field saturation, followed by reorientation, motion and distortion correction, skull stripping, and nuisance variable removal using FIX (Salimi-Khorshidi et al., 2014). Functional time series were mapped to each

individual's cortical surface using boundary-based registration and subsequently to the 32k vertex Conte69 template.

## 2.4. Structural connectome generation and manifold identification

Structural connectomes were generated from preprocessed dMRI data using MRtrix (Tournier et al., 2019, 2012). Different tissue types of cortical and subcortical grey matter, white matter, and cerebrospinal fluid were segmented using T1-weighted image for anatomical constrained tractography (Smith et al., 2012). Multi-shell and multi-tissue response functions were estimated (Christiaens et al., 2015) and constrained spherical-deconvolution and intensity normalization were performed (Jeurissen et al., 2014). The initial tractogram was generated with 40 million streamlines, with a maximum tract length of 250 and a fractional anisotropy cutoff of 0.06. Spherical-deconvolution informed filtering of tractograms (SIFT2) was applied to reconstruct whole brain streamlines weighted by cross-section multipliers (Smith et al., 2015). To build a structural connectome, the reconstructed cross-section streamlines were mapped onto the Schaefer atlas with 200 parcels (Schaefer et al., 2018). Connectome data were log-transformed to reduce connectivity strength variance (Fornito et al., 2016; Goñi et al., 2014).

The principal eigenvectors explaining spatial shifts in the structural connectome, referred to as *structural connectome gradients* were estimated using the BrainSpace toolbox (<https://github.com/MICA-MNI/BrainSpace>) (Margulies et al., 2016; Vos de Wael et al., 2020). A cosine similarity matrix was constructed from the group averaged structural connectome to capture the similarity of connections among different brain regions. We capitalized on diffusion map embedding, a non-linear manifold learning algorithm, to identify low dimensional manifolds (i.e., principal components) (Cox, 1996). In this manifold, strongly interconnected brain regions that have many and/or strong connections are closely located, while regions with little and/or weak inter-connectivity are farther apart. Diffusion map embedding algorithm is robust to noise and computationally efficient compared to other non-linear manifold learners (Tenenbaum et al., 2000; Von Luxburg, 2007). The algorithm is controlled by two parameters  $\alpha$  and  $t$ , where  $\alpha$  controls the influence of the density of sampling points on the manifold ( $\alpha = 0$ , maximal influence;  $\alpha = 1$ , no influence) and  $t$  controls the scale of eigenvalues of the diffusion operator. We followed recommendations and fixed  $\alpha$  at 0.5 and  $t$  at 0, a choice that retains the global relations between data points in the embedded space (Hong et al., 2019; Margulies et al., 2016; Paquola et al., 2019; Vos de Wael et al., 2018).

## 2.5. Dynamic functional connectivity analysis

Dynamic functional connectivity analysis was performed using a multivariate autoregressive HMM approach, which models distinct brain states via a multivariate Gaussian distribution and which infers model parameters via variational Bayes (<https://github.com/OHBA-analysis/HMM-MAR>) (Vidaurre et al., 2017). The number of brain states was determined according to the following six steps: (1) For each participant, we divided the functional time series into ten non-overlapping segments and (2) applied k-means clustering to 9/10 time series segments with  $k$  ranging from 2 to 20. (3) For each  $k$ , we calculated the ratio of between-cluster variance to total variance, and the optimal number of brain states for the given time series was determined as the minimum value at which the explained variance exceeded 90% of total variance (Kodinariya and Makwana, 2013; Park et al., 2018b). (4) We repeated steps 1–3 for a total of 10 times with different time segments within a participant, and (5) also repeated steps 1–4 for all participants. (6) Finally, we determined the optimal number of brain states for HMM training as the most frequently observed number of  $k$  across time segments and participants. We trained HMM using the concatenated time series across participants. To mitigate circularity (Kriegeskorte et al., 2009), we used different time

segments for HMM training and brain state estimation. For each participant, we concatenated 50% of the time series from session 1 and the other 50% from session 2. Then, we concatenated this reconstructed time series across all participants to train the HMM. The trained model was applied to the rest of the time series to estimate distinct brain states. HMM estimates specific states, where a state  $k$  is characterized by a multivariate Gaussian distribution with a mean distribution of whole-brain activity ( $\mu_k$ ) and covariance matrix ( $\Sigma_k$ ) (Vidaurre et al., 2018, 2017). Specifically, time series data  $x$  in the hidden state  $s$  at time  $t$  follows the multivariate Gaussian distribution  $N$  as follows:

$$x_t | s_t = k \sim N(\mu_k, \Sigma_k) \quad (1)$$

Here,  $\mu_k$  is a vector of mean blood oxygen level-dependent (BOLD) activation, which is here referred to as functional mean patterns of activation (fMPA), and  $\Sigma_k$  is the covariance matrix when state  $k$  is active. In addition, HMM estimates transition probabilities between brain states and allows representing the frequency of transitions (Vidaurre et al., 2018, 2017). Meta-states, i.e., communities of functional states, were estimated to simplify the transition structure (Vidaurre et al., 2017), by applying the Louvain community detection algorithm (Blondel et al., 2008) to the transition probability matrix. To avoid effects related to random HMM initialization, HMM training, estimating brain states, and meta-state estimation were repeated 100 times. The most frequently observed meta-state structure across iterations was selected.

## 2.6. Association between functional dynamics and structural connectome organization

Structure-function coupling was first assessed by spatial associations (i.e., linear product moment correlation coefficients) between structural gradients and differences in fMPA ( $\Delta$ fMPA) within and between meta-states. Specifically, we calculated  $\Delta$ fMPA as the average of differences in fMPA between all possible pairs of transitions within or between meta-states:

$$\Delta fMPA_{\{S \rightarrow T\}} = \frac{1}{A} \sum_{i=1}^N \sum_{j=1}^M fMPA_{S_i} - fMPA_{T_j} \quad (2)$$

Here,  $i$  and  $j$  are individual states within meta-states  $S$  and  $T$ ;  $N$  and  $M$  are the numbers of individual states in the meta-states; and  $A$  is the number of possible pairs of state transitions (i.e., transitions within meta-state:  $A = {}_N C_2$ , transitions between meta-states:  $A = N \cdot M$ ). The significance of the correlation was assessed using 1,000 spin tests, which randomly rotate  $\Delta$ fMPA and hence preserve the spatial autocorrelation (Alexander-Bloch et al., 2018). A null distribution was constructed, and the real correlation strength was deemed significant if it belonged to the 5<sup>th</sup> percentile. To evaluate whether the above structure-function associations were robust above and beyond inter-regional variations of cortical morphology, we correlated  $\Delta$ fMPA with MRI-derived cortical thickness and folding measures (derived from FreeSurfer). In addition, we controlled for cortical thickness and folding when correlating  $\Delta$ fMPA with structural connectome gradients, to establish that structural gradients explain dynamic functional shifts above and beyond the effects of cortical morphology.

## 2.7. Associations of functional dynamics with network topology

To assess structural network topology underpinnings of distinct functional dynamic states, we stratified  $\Delta$ fMPA in terms of rich-club taxonomy, a topological measure sensitive to core-periphery organization of the network (Griffa and van den Heuvel, 2018; van den Heuvel et al., 2012). The rich-club is a set of highly interconnected high-degree nodes. It has been shown to play an important role in information integration between different brain networks and aggregates

most long-range connections of the human brain (de Reus and van den Heuvel, 2013; Griffa and van den Heuvel, 2018; Liang et al., 2018; Shu et al., 2018; van den Heuvel et al., 2012; Zhao et al., 2017). In contrast, peripheral nodes show shorter, more local connections and serve in more specialized, segregated functions (de Reus and van den Heuvel, 2013; Griffa and van den Heuvel, 2018; Liang et al., 2018; Shu et al., 2018; van den Heuvel et al., 2012; Zhao et al., 2017). The weighted rich-club coefficient  $\varphi^W(k)$  was calculated from the group representative structural connectome, defined using a distance-dependent thresholding (Betzel et al., 2019), using the Brain Connectivity Toolbox (<https://sites.google.com/site/bctnet/>) (Rubinov and Sporns, 2010). The  $\varphi^W(k)$  was calculated across different levels of degree ( $k$ ) ranging from 1 to the maximal degree and was normalized against 1,000 randomly rewired networks with similar degree distribution. Degree levels in which (i) the normalized rich-club coefficient exceeded one (i.e.,  $\varphi^W_{norm}(k) > 1$ ) and (ii) where there were significant differences between real and randomized networks ( $p < 0.05$ , permutation test corrected) were considered as the rich-club regime. The rich-club nodes were defined as nodes exceeding the  $k^{\text{th}}$  degree level in the rich-club regime (here,  $k = 28$ ). Remaining nodes were classified into *feeder* nodes, which had more than 10% connections with rich-club nodes, and *local* nodes, which had less than 10% connections (Hong et al., 2019). The magnitude of  $\Delta$ fMPA within and between meta-states was quantified according to the rich-club taxonomy and they were compared using two-sample t-tests across rich-club, feeder, and local nodes. Findings were corrected at a false discovery rate  $<0.05$  (Benjamini and Hochberg, 1995).

Structural connectivity distance provides an index of network hierarchy complementary to rich-club taxonomy, given the observation that backbone hubs often host longer-range connections to distributed targets than local nodes that mostly travel along short-range paths (Avena-Koenigsberger et al., 2019; van den Heuvel et al., 2012). To assess the relationship between functional dynamic transitions and structural connectivity distance, we stratified  $\Delta$ fMPA according to connectivity distance (Larivière et al., 2019b; Oligschläger et al., 2019). Connectivity distance, thus, indicates a given brain area's average geodesic distance to its structurally connected regions (Oligschläger et al., 2019). Geodesic distance was defined as the shortest path connecting two points along the cortical surface, following prior procedures (Ecker et al., 2013; Hong et al., 2018; Margulies et al., 2016). It represents the physical distance between the two cortical points when travelling through the cortical sheet, and does not depend on network topology. The multiplication between the geodesic distance and the binarized structural connectome was performed, and the row-wise mean was calculated to compute the connectivity distance (Hong et al., 2019; Oligschläger et al., 2019). The connectivity distance was partitioned into 10 bins and the magnitude of  $\Delta$ fMPA was quantified according to each bin.

## 2.8. Role of network communication

In addition to the rich-club taxonomy and connectivity distance measures, we leveraged network communication models that determine how a structural connectome can implement functional signaling and information transfer (Avena-Koenigsberger et al., 2019, 2018; Goñi et al., 2014) to associate functional dynamics to models of structurally-governed communication (Avena-Koenigsberger et al., 2018; Goñi et al., 2014). The metrics of mean first-passage time and path length measuring network diffusivity (Avena-Koenigsberger et al., 2018) were calculated from the weighted structural connectivity matrix using the Brain Connectivity Toolbox (<https://sites.google.com/site/bctnet/>) (Rubinov and Sporns, 2010). Mean first-passage time quantifies the expected length of a random walk between two nodes, indicating a diffusion mechanism (Avena-Koenigsberger et al., 2018; Goñi et al., 2013). Path length, on the other hand, is defined as the shortest weighted path between the source and target; nodes with low path lengths contribute to globally efficient communication (Avena-Koenigsberger et al.,

2018; Goñi et al., 2014; Rubinov and Sporns, 2010). To assess differences in communication mechanisms of the brain regions showing large changes in brain activity during meta-state transitions, we quantified mean first-passage time and path length in the brain regions, which showed a strong (top 5%) magnitude of  $\Delta fMPA$  within and between meta-states, and computed communication metrics on resultant submatrices. We repeated calculating mean first-passage time and path length in the brain regions that showed the top 10, 15, and 20% magnitude of  $\Delta fMPA$  within and between meta-states to assess the consistency of the findings. To confirm findings using alternative parameters, we additionally stratified changes in  $\Delta fMPA$  with respect to search information and path transitivity (Avena-Koenigsberger et al., 2018; Goñi et al., 2014). Search information quantifies the amount of information needed to access the path connecting from a source node to a target node (Avena-Koenigsberger et al., 2018; Goñi et al., 2014). Similar to mean first-passage time, higher search information indicates the diffuse property of the network by implying that it requires a large amount of information to reach the target node through the shortest path (Avena-Koenigsberger et al., 2018; Goñi et al., 2014). Path transitivity captures the density of local detours along the given shortest path, indicating high path transitivity represents the existence of many closed loops along the path enabling a signal to return to the shortest path after detouring (Avena-Koenigsberger et al., 2018; Goñi et al., 2014).

### 2.9. Functional dynamic transitions in terms of cortical hierarchy

Finally, we contextualized functional dynamic transitions within a prior model of neural organization formulated in non-human primates that subdivides the cortex into four levels: idiosyncratic (level-1), unimodal association (level-2), heteromodal association (level-3), and paralimbic (level-4) cortices (Mesulam, 1998). Hierarchical weights of the fMPA patterns for each state were quantified with respect to Mesulam hierarchy for each brain state. The discretized fMPA was interpolated with 30 bins and the point that exhibited maximum fMPA value was selected as the mean hierarchical level. For each hierarchical level, we calculated the following topological parameters and communication metrics: (i) the proportion of rich-club nodes (relative to all nodes on that hierarchical level), (ii) the average connectivity distance, and (iii) ratio between signal diffusion to routing in terms of structurally-governed communication. For diffusion/routing communication ratio, we calculated the ratio between mean first-passage time and path length. The linear product moment correlation between the first structural gradient (sG1) and  $\Delta fMPA$  and mean hierarchical level between all pairs of brain states were computed. Then, the magnitude of structure-function coupling (*i.e.*, correlation between sG1 and  $\Delta fMPA$ ) was quantified according to the mean hierarchical level to assess the relationship between cortical hierarchy and structure-functional dynamic coupling.

### 2.10. Sensitivity and reproducibility analyses

- Matrix thresholding.** We repeated structural gradient estimation based on structural connectomes with different levels of density (unthresholded, 25, 50, and 75% density).
- Spatial scale.** To evaluate the impact of spatial scale, we repeated our analyses across different granularities of the Schaefer atlas (*i.e.*, 100, 300, or 400 regions) (Schaefer et al., 2018).
- Reproducibility in HCP.** We assessed reproducibility by performing the same analyses on the independent Replication subset from the HCP. Structural gradients, functional brain states, and the correlation between structural gradients and  $\Delta fMPA$  as well as morphological associations were computed and compared to those in the Discovery cohort.
- Reproducibility in another dataset.** We furthermore replicated our findings in a locally scanned cohort (MICA-MTL, n = 47).

## 3. Results

### 3.1. Cortex-wide structural connectome gradients

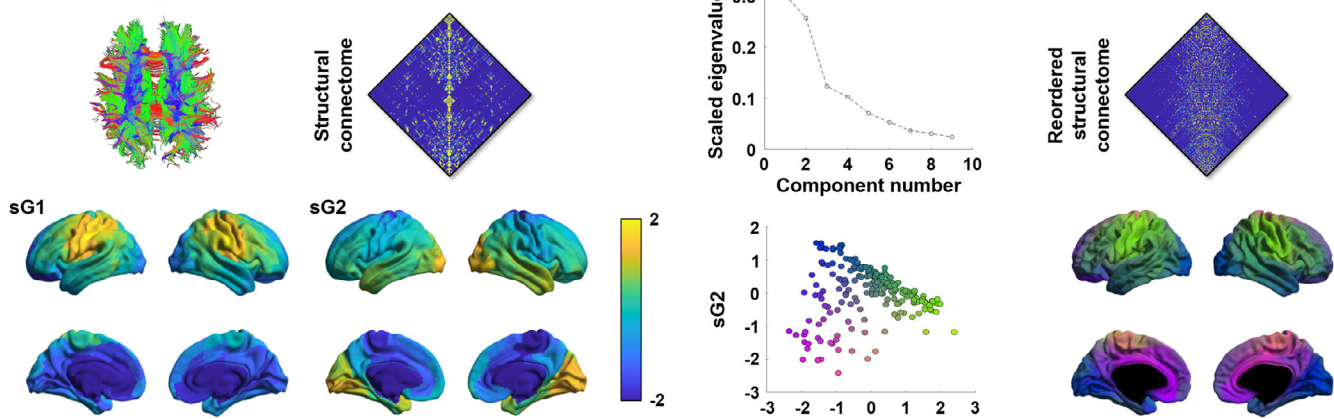
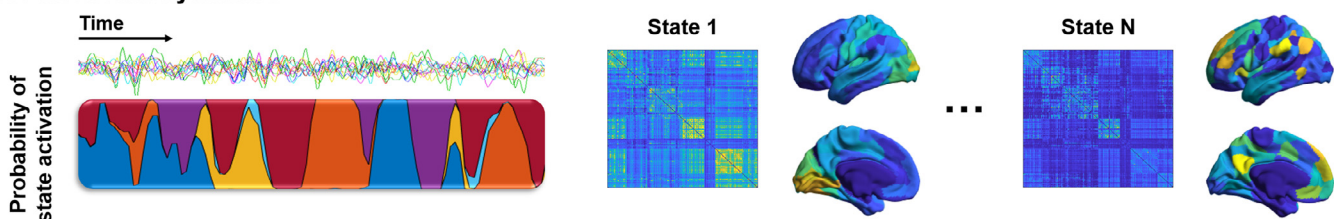
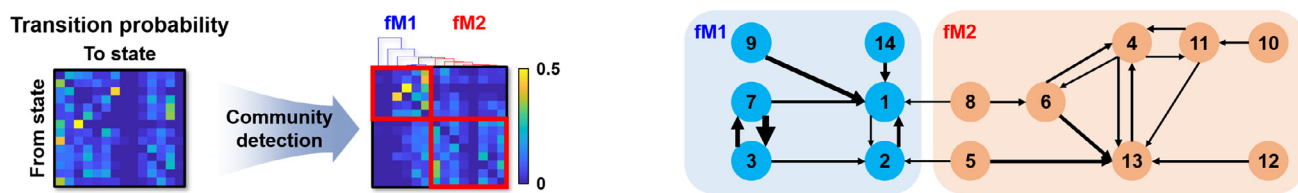
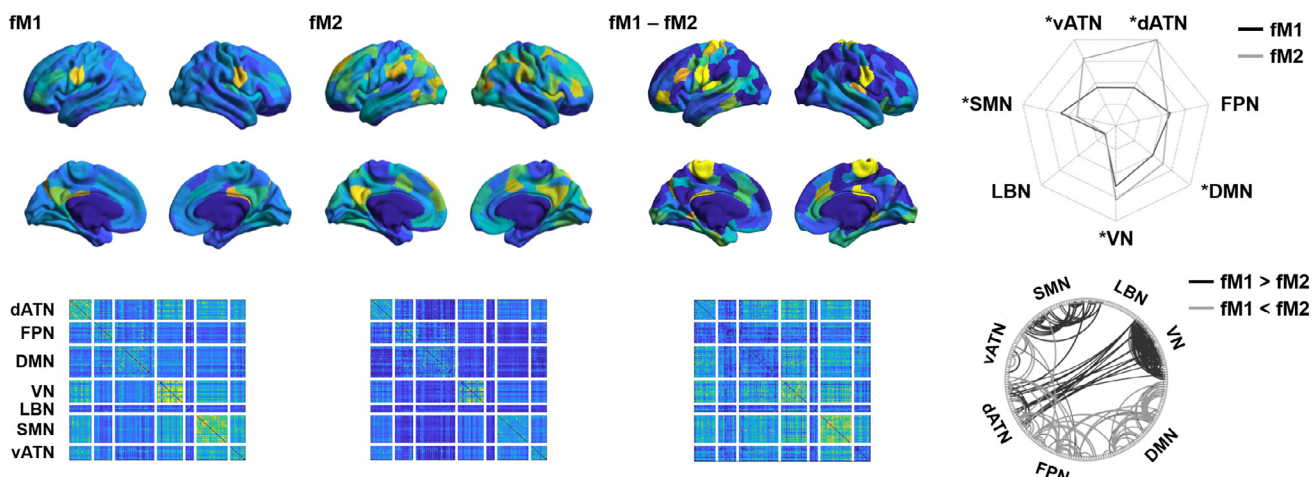
We computed whole brain structural connectomes from all participants, using an established parcellation scheme (See *Supporting Information* for replication across partitioning schemes and spatial scales) (Schaefer et al., 2018). Using non-linear dimensionality reduction techniques, we derived structural connectome gradients (Vos de Wael et al., 2020). The first two gradients (sG1, sG2) were selected, as these explained 44.5% of connectome variance and corresponded to the clearest elbow in the scree plot (Fig. 1A). For additional information, the third to fifth gradients (sG3, sG4, sG5) are shown in Fig. S1A but will not be further discussed. While sG1 differentiated a sensorimotor from a medial prefrontal anchor, sG2 extended from the ventral to dorsal visual systems. Structural gradients were consistent across different levels of density in structural connectomes, which showed mean product moment correlations across spatial maps of 0.95 with SD 0.03 ( $p < 0.001$ ) (Fig. S1B).

### 3.2. Dynamic functional connectivity analysis

Dynamic changes in functional states were estimated using an HMM (Fig. 1B). HMM provided the fMPA and associated connectivity matrix for each brain state (Fig. S2A), as well as transition probabilities between states. Meta-states were estimated to simplify the transition structure (Vidaurre et al., 2017) via Louvain community detection (Fig. 1C) (Blondel et al., 2008). This approach identified two functional meta-states fM1 and fM2, each with distinct spatial activation and connectivity patterns. fM1 showed high activation in sensorimotor and lateral prefrontal regions while fM2 showed activations in default and frontoparietal networks (Fig. 1D). Spatial correlations in activation patterns between both meta-states were low (mean  $\pm$  SD  $r = 0.24 \pm 0.10$ ), while states falling within each meta-state showed moderate to high correlations to one another (mean  $\pm$  SD  $r = 0.32 \pm 0.17$  for fM1 and  $r = 0.36 \pm 0.19$  for fM2). Directly comparing the top 1% connections between meta-states, fM1 had stronger connections in visual and somatosensory networks, and fM2 showed stronger connections in frontoparietal and default-mode networks (Table S1). Furthermore, the correlation between fMPA of meta-states and meta-analysis maps of diverse cognitive domains (Margulies et al., 2016), derived using Neurosynth (Yarkoni et al., 2011), revealed distinct cognitive term associations between meta-states; fM1 was characterized by ‘motor’ terms while fM2 related to higher-order cognitive terms such as ‘autobiographical memory’ and ‘social cognition’ (Fig. S2B). Collectively, these findings support that fM1 reflects a low-level sensorimotor state whereas fM2 is more involved in higher-order transmodal functions.

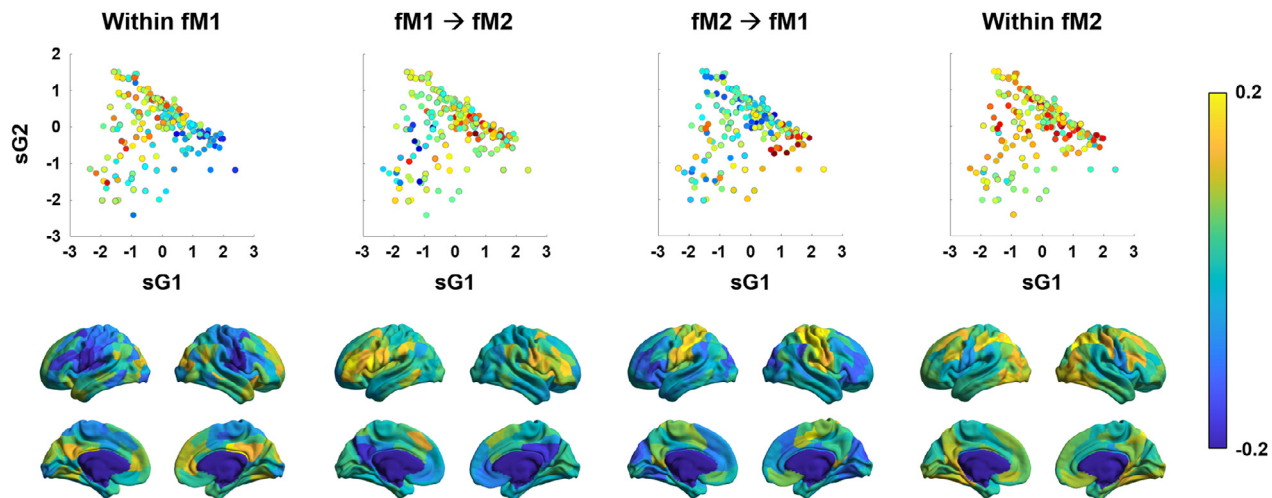
### 3.3. Structural connectome gradients relate to dynamic functional transitions

To assess structure-function correspondence, we computed product moment correlations between structural connectome gradients sG1 and sG2 and dynamic activity changes ( $\Delta fMPA$ ) within the two meta-states fM1 and fM2, and between them. Activity changes for all transitions involving fM1 were correlated with sG1 but not sG2, with significance determined using non-parametric spin tests that adjust for shared spatial autocorrelations (Fig. 2 and Fig. S3) (Alexander-Bloch et al., 2018; Vos de Wael et al., 2020). Indeed, sG1 correlated with transitions within fM1 ( $r = -0.5778$ ,  $p < 0.001$ ), from fM1 to fM2 ( $r = 0.3827$ ,  $p < 0.05$ ), and from fM2 to fM1 ( $r = 0.4635$ ,  $p < 0.005$ ). Conversely, no significant relationship was found in transitions within fM2 ( $r = 0.0758$ ,  $p > 0.4$ ). Although sG2 by itself did not significantly correlate with these transitions, model fit (*i.e.*, adjusted  $R^2$ ) generally improved when incorporating both sG1 and sG2 into a common model via linear regression (+4.1% variance explained for transitions within fM1; +2.4% from fM1

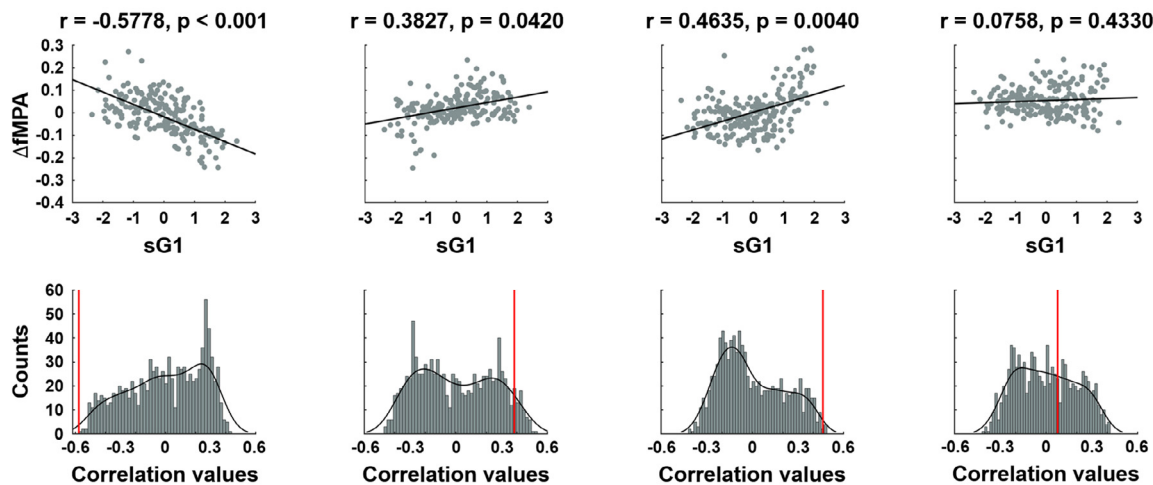
**A. Structural gradients****B. Functional dynamics****C. Metastates****D. fMPA and connectivity**

**Fig. 1.** Structural gradients and dynamic functional connectome profiles. (A) Manifolds estimated from the structural connectome. Systematic dMRI fiber tracking generated a cortex-wide structural connectome, on which non-linear dimensionality reduction identified principal components describing connectivity variance. The first two components (sG1 and sG2) corresponded to the clearest elbow in the scree plot. (B) Dynamic functional analysis leveraged Hidden Markov Models (HMM) that decompose the time series into a set of states and their transition probabilities. (C) Transition probabilities were clustered using a community detection algorithm to identify functional meta-states (fM1 and fM2). Line widths represent transition probability strengths, thresholded at 0.2. (D) The functional mean patterns of activation (fMPA) for two meta-states (fM1, fM2) and their differences at the level of the whole brain and functional networks are shown in the upper row. Significant differences in fMPA between fM1 and fM2 are indicated with an asterisk. Corresponding connectivity matrices and differences in edges with top 1% weights for the two meta-states are shown in the bottom row. Abbreviations: dATN, dorsal attention network; FPN, frontoparietal network; DMN, default-mode network; VN, visual network; LBN, limbic network; SMN, sensorimotor network; vATN, ventral attention network.

### A. Structural gradients and $\Delta fMPA$



### B. Correlation between sG1 and $\Delta fMPA$



### C. Correlation between sG1+sG2 and $\Delta fMPA$

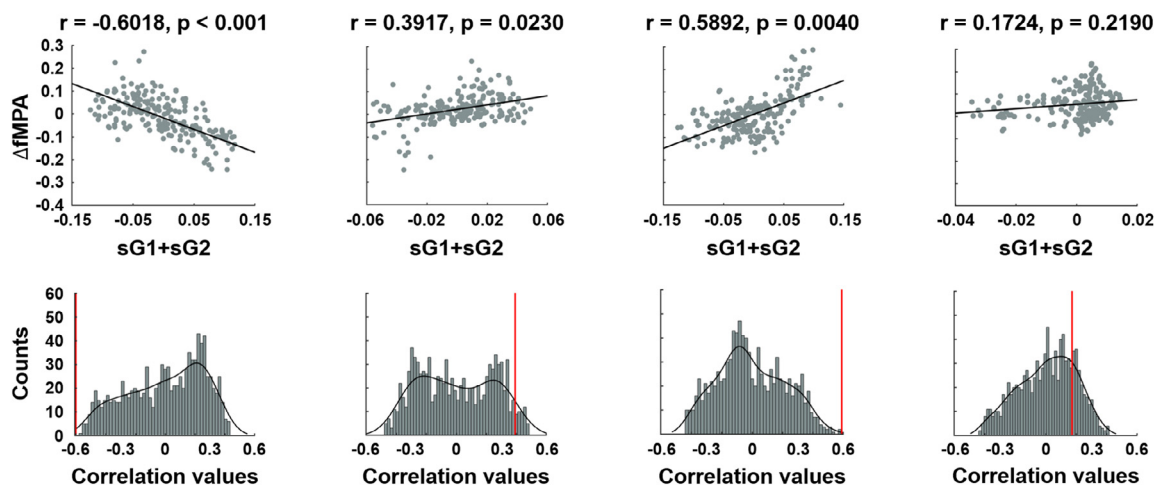


**Fig. 2.** Associations between structural gradients and functional dynamic transitions. (A) The  $\Delta fMPA$  with respect to sG1 and sG2 were reported in the upper row. The color indicates the magnitude of  $\Delta fMPA$ . The  $\Delta fMPA$  for transitions within and between meta-states are reported in the bottom row. (B) The correlation between sG1 and  $\Delta fMPA$ . Permutation-based correlation values across 1,000 spin tests are shown in the histogram, with the real correlation value indicated via a red line. (C) Linear fit of  $\Delta fMPA$  using both sG1 and sG2, incorporated via linear regression model.

to fM2; +27.1% from fM2 to fM1; and +127.4% within fM2). For transitions within fM1 and from fM2 to fM1, both sG1 and sG2 showed significant contributions for model fitting (within fM1:  $p < 0.001/0.0035$  for sG1/sG2; from fM2 to fM1:  $p < 0.001/< 0.001$ ). On the other hand, only sG1 showed significance for the transitions between fM1 to fM2 ( $p < 0.001/0.2059$ ), and only sG2 showed significance for the transitions within fM2 ( $p = 0.2859/0.0285$ ).

### 3.4. Morphological structures are not relevant to functional dynamic transitions

To assess contributions of regional morphological variations, we also correlated MRI-derived measures of cortical thickness and folding to  $\Delta fMPA$ . We observed weak and non-significant associations with cortical thickness (Fig. 3A). Although the association between cortical folding and activity changes within fM1 and from fM2 to fM1 reached significance, correlations were overall relatively weak (Fig. 3B). Importantly, the correlations between structural gradients and  $\Delta fMPA$  were robust after correcting gradient values for cortical thickness and folding, both for the model based on sG1 only (Fig. 3C) and for the model based on both sG1 and sG2 (Fig. 3D), suggesting that structural connectome organization contains information about neural dynamics above and beyond the information provided by local variation in cortical morphology.

### 3.5. Connectome topology analysis

The above findings suggest a reasonably strong structure-function correspondence for functional transitions involving states anchored in sensorimotor systems (*i.e.*, within fM1, from fM1 to fM2, and from fM2 to fM1). However, there was no comparable prediction for states that are linked to more transmodal regions. These findings are broadly in line with previous findings showing stronger structure-function coupling in unimodal than transmodal cortices (Park and Friston, 2013; Vázquez-Rodríguez et al., 2019). To understand the underlying mechanism of flexibility in more transmodal states, we next evaluated the relationship to network topology parameters describing long distance communication between regions (Avena-Koenigsberger et al., 2019, 2018). Contemporary views of cortical organization have highlighted that the cortex is organized by an apparent rich-club structure, in which certain hub regions are more densely connected to themselves than to the rest of the brain (Avena-Koenigsberger et al., 2019, 2018; Bullmore and Sporns, 2009; van den Heuvel et al., 2012). We identified the rich-club following established procedures (Fig. 4A). Rich-club nodes were located at backbone structures and surrounded by feeder nodes, and local nodes were located near sensorimotor areas (Fig. 4A). Notably, high  $\Delta fMPA$  was observed in local nodes for the transitions within fM1 and from fM2 to fM1, while no differences were found within fM2 and from fM1 to fM2, indicating that the transitions in sensorimotor-dominated states primarily occurred in the locally-connected brain regions and those in transmodal states occurred uniformly across either local or hub nodes.

As a complementary information to rich-club taxonomy, we stratified  $\Delta fMPA$  according to structural connectivity distance (Larivière et al., 2019b; Oligschläger et al., 2019). Stratifying dynamic functional changes ( $\Delta fMPA$ ) with respect to connectivity distance, we observed that transitions within fM1 or from fM2 to fM1 more frequently involved short-range connections, while those within fM2 or from fM1 to fM2 involved long-range connections (Fig. 4B). Shifts in  $\Delta fMPA$  according to connectivity distance indicate that marked transitions occurred along with the short-range connections for low-level brain states, while transitions for the higher-order brain state increasingly used long-range connections. Our results indicate that transitions involving sensorimotor states traverse along the path with short distances, while those in transmodal states engage long-range connections across network hubs.

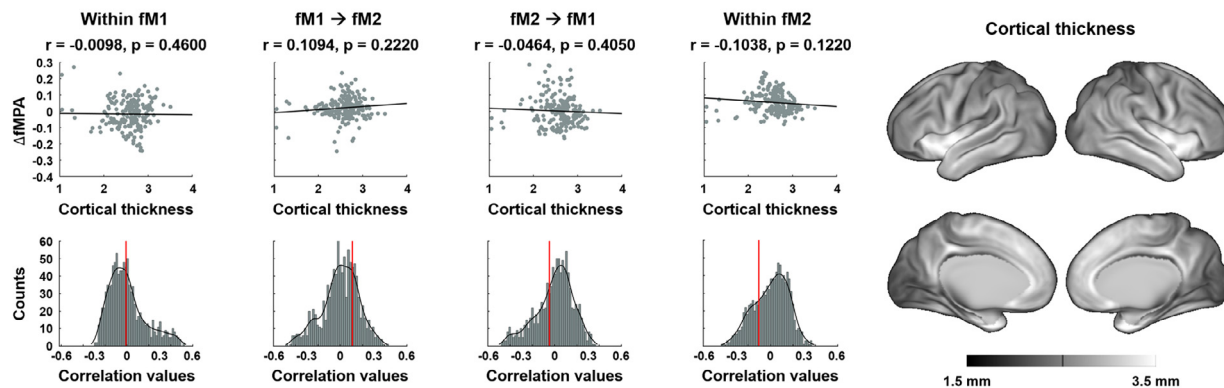
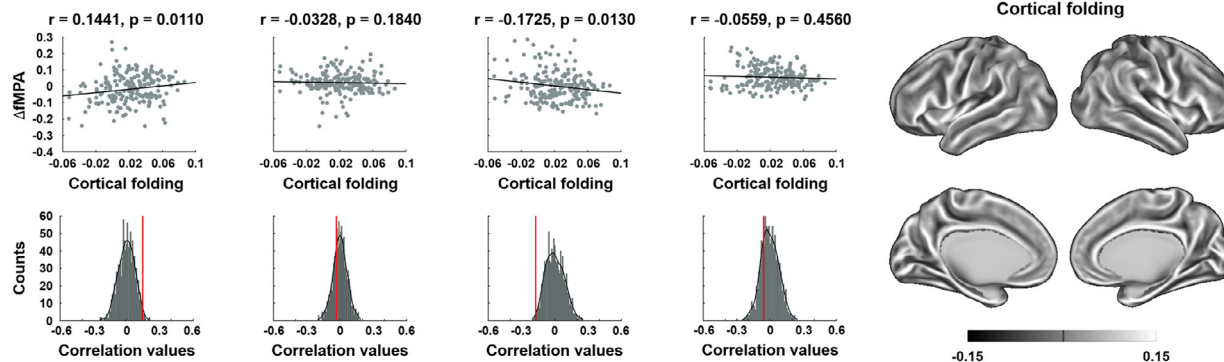
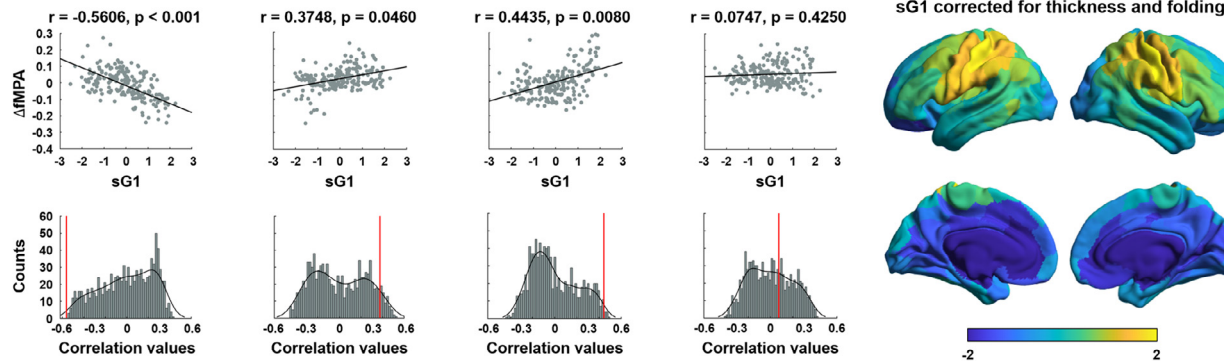
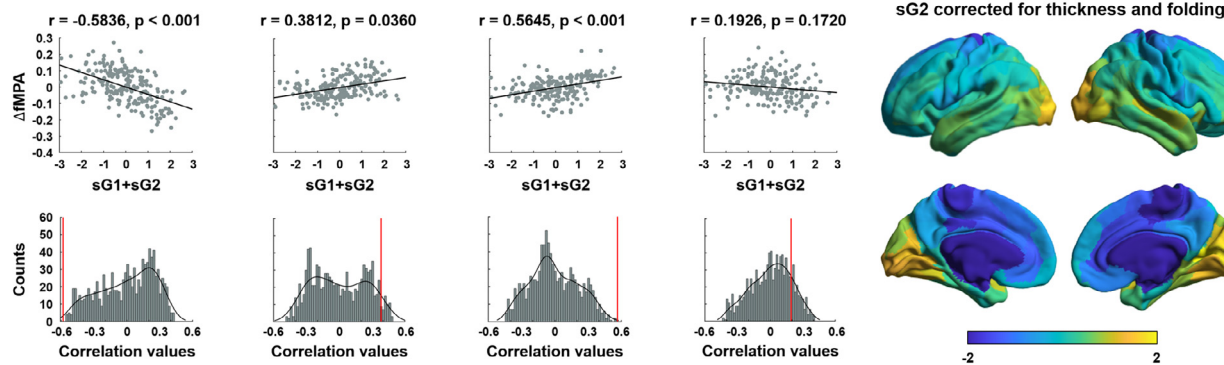
We furthermore derived mean first-passage time and path length from the structural connectome to assess structurally-governed network communication (Avena-Koenigsberger et al., 2018; Goñi et al., 2014). Interestingly, higher mean first-passage time was observed in transitions within fM1 and from fM2 to fM1 compared to transitions from fM1 to fM2 and within fM2. Similarly, higher path length was observed within fM1, and it monotonically decreased in transitions between meta-states and within fM2 (Fig. 4C). This analysis indicates different functional states are associated to different structural communication mechanisms. Specifically, communication in functional states localized in low-level sensory areas is better explained by network diffusion. On the other hand, functional states in transmodal regions are better explainable by routing along shortest paths. Results for mean first-passage time and path length were consistent when considering those brain regions of the top 10, 15, and 20%  $\Delta fMPA$  within and between meta-states (Fig. S4). To further validate our findings using different graph parametrization methods, we calculated search information and path transitivity. Higher search information was observed in transitions within fM1 and monotonically decreased in transitions between meta-states and within fM2. In contrast, higher path transitivity was observed within fM2 and in transitions from fM1 to fM2 compared to fM1 (Fig. S5), suggesting consistent results with mean first-passage time and path length.

### 3.6. Cortical hierarchy and functional dynamic transitions

To assess how the dynamic fluctuations of brain function change according to contemporary views of cortical hierarchy (Fig. 5A), we first computed the mean hierarchical level for each brain state based on hierarchical system proposed by Marcel Mesulam (Mesulam, 1998). Brain states in fM1 had a tendency for lower mean hierarchical levels than those in fM2 (mean  $\pm$  SD =  $1.70 \pm 1.10$  vs.  $2.61 \pm 1.14$ ;  $t = -1.50$ , one-tailed  $p = 0.08$ ). Although the difference was not statistically significant, this suggests that both meta-states may be involved in different hierarchical levels, where dynamic functional states in fM1 were anchored in lower levels of the hierarchy, while those in fM2 were anchored in higher levels (Fig. 5B). We aimed to understand the specific features of cortical topology that underpinned this relationship by calculating the proportion of rich-club nodes, connectivity distance, and diffusion/routing communication ratio (*i.e.*, ratio between mean first-passage time and path length) within each of the four levels of the hierarchy. Confirming the differentiation of our structure-function relationships across the hierarchy, we observed a higher proportion of rich-club nodes and longer connectivity distance in higher-order regions, together with lower diffusion/routing communication ratio (Fig. 5C). Importantly, beyond the location of states in the hierarchy, the magnitude of structure-function coupling (*i.e.*, correlation between sG1 and  $\Delta fMPA$ ) was strong when dynamic states changed within the low hierarchical levels, between low- and high-level hierarchies, while the coupling appeared weakest for dynamic transitions between high level states (Fig. 5D). Together, this result supports our finding that structure-function correspondence is strong when dynamic transitions involve sensorimotor states and that correspondence decreases when transitions are anchored in transmodal states.

### 3.7. Sensitivity and replication experiments

Repeating the above analysis across spatial scales (*i.e.*, 100, 300, and 400 parcels), findings were highly consistent at parcel resolutions  $> 100$  (Fig. S6–8). Correlations between sG1 and  $\Delta fMPA$  became somewhat weaker at the lowest resolution of 100 parcels, indicating that more granular parcellations may be more efficient for the study of associations between structural connectivity and functional dynamics. To assess reproducibility, we performed the same analyses on the initially held out Replication dataset from the HCP. We observed virtually identical patterns of structural connectome gradients, functional meta-states, and structure-function associations (Fig. S9–10). Finally, main findings

**A. Correlation between cortical thickness and  $\Delta fMPA$** **B. Correlation between cortical folding and  $\Delta fMPA$** **C. Correlation between  $\Delta fMPA$  and sG1 corrected for thickness and folding****D. Correlation between  $\Delta fMPA$  and sG1 and sG2 corrected for thickness and folding**

**Fig. 3.** Morphological associations. (A) Correlations between cortical thickness and  $\Delta fMPA$ , showing scatter plots and spin test histograms. (B) Correlations between cortical folding and  $\Delta fMPA$ . (C) Correlations between  $\Delta fMPA$  and sG1, corrected for cortical morphology. (D) Linear model between  $\Delta fMPA$  and sG1 and sG2, corrected for cortical morphology.

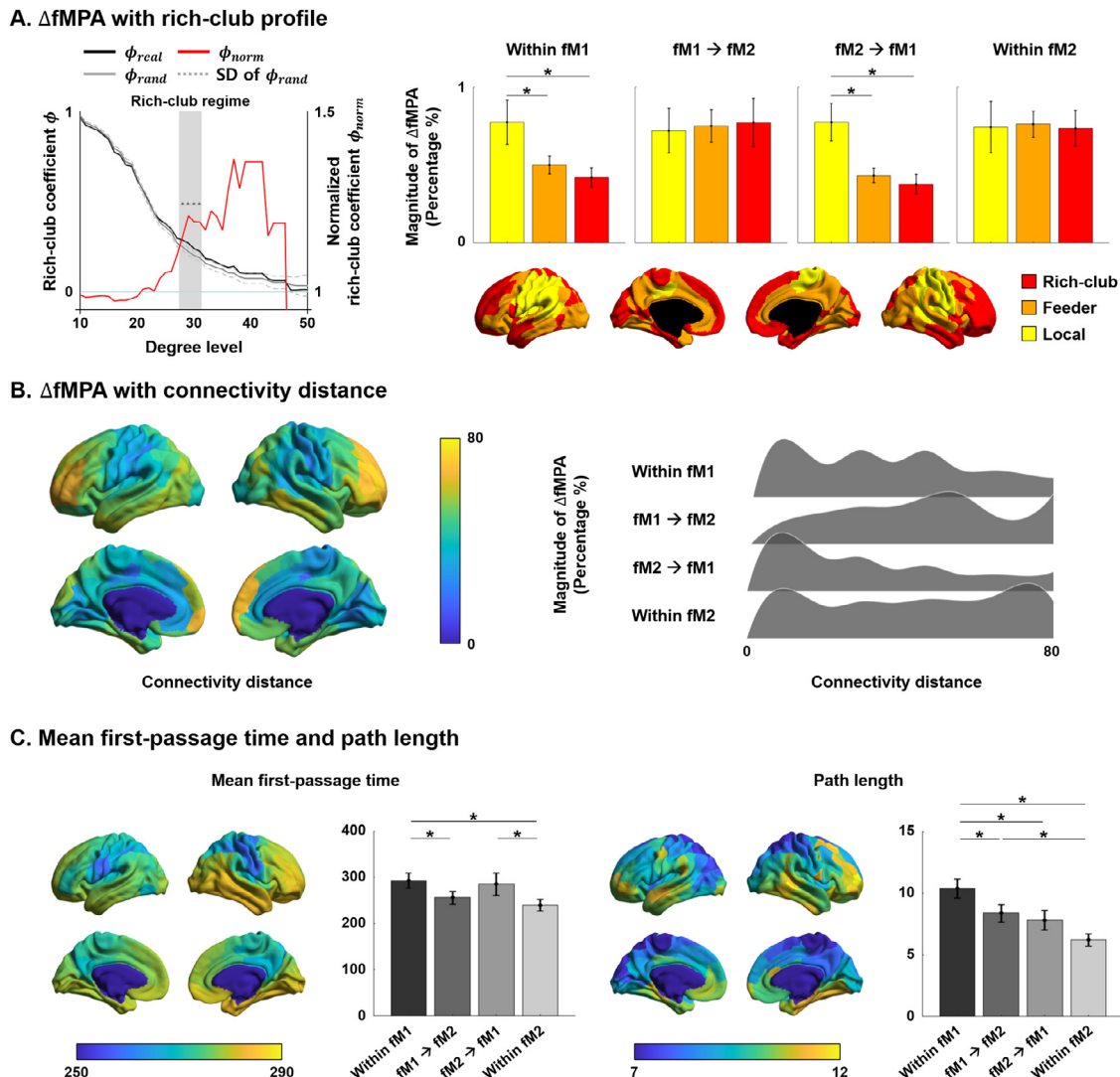


**Fig. 4.** Connectome topology analysis. (A)  $\Delta f\text{MPA}$  in terms of rich-club taxonomy. Rich-club coefficients according to different degree levels were reported on the left side and the magnitudes of  $\Delta f\text{MPA}$  of rich-club, feeder, and local nodes were reported on the right side. The error bars represent the standard deviation of  $\Delta f\text{MPA}$  across brain regions. (B)  $\Delta f\text{MPA}$  in regard to connectivity distance. The connectivity distance was reported on the left side and the magnitudes of  $\Delta f\text{MPA}$  according to the connectivity distance were reported on the right side. (C) Mean first-passage time and path length with respect to the meta-state transitions. The error bars indicate the standard deviation of network communication measures across transitions.

could be confirmed in the independent 3T dataset from our local site that had slightly different imaging parameters as HCP (MICA-MTL) (Fig. S11).

#### 4. Discussion

Understanding how the structure of the cortex gives rise to ongoing cognitive function is a key aim for systems neuroscience (Batista-García-Ramó and Fernández-Verdecia, 2018; Baum et al., 2020; Becker et al., 2018; Ceric et al., 2017; Hermundstad et al., 2013; Honey et al., 2009; Mišić et al., 2016; Park and Friston, 2013; Rubinov et al., 2009; Snyder and Bauer, 2019; Suárez et al., 2020; Vázquez-Rodríguez et al., 2019; Wang et al., 2019, 2015). Yet, it remains unclear how a hard-wired neural architecture can give rise to flexible (*i.e.*, time-varying) neural dynamics. Our analysis established that low dimensional representations of white matter connectivity are closely aligned with spatiotemporal patterns of dynamic functional transitions between lower-level sensorimotor states, and between lower-level and higher-order transmodal states. Conversely, transitions between states anchored in transmodal regions were not simply explained by structural connectome

organization. This apparent difference may occur because transitions between transmodal states preferentially related to subnetworks that communicate increasingly via a routing strategy involving long-range and globally efficient connections. In contrast, sensorimotor state changes were primarily explicable in terms of changes through local network diffusion and implicated shorter connectivity distances. Findings were robust across multiple sensitivity analyses and could be replicated in different datasets. Together, our work suggests that flexible neural dynamics may rely on a balance between complementary features of structural connectome organization: Local aspects of brain structure are important for shifts between neural states anchored in sensorimotor cortex, and a more distributed rich club architecture support transitions between neural states anchored in transmodal cortex.

Our study capitalized on manifold learning techniques applied to structural connectome data, an approach that has recently gained traction in the neuroimaging and network neuroscience communities, as it offers novel perspectives on dimensions of brain organization giving rise to human cognition (Margulies et al., 2016; Vos de Wael et al., 2020). While similar algorithms have been applied to microstructural and functional connectivity data (Burt et al., 2018; Huntenburg et al.,

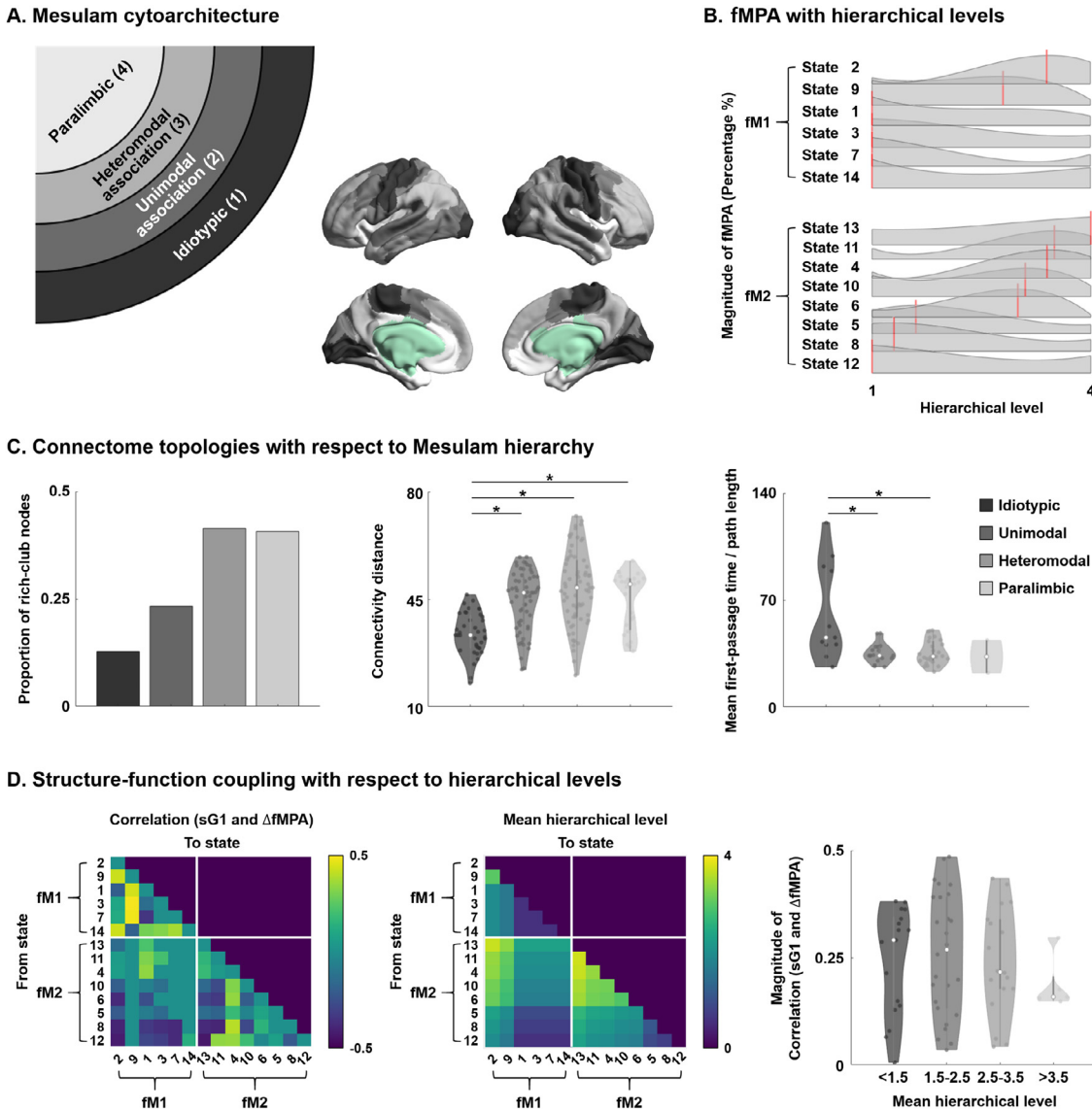


**Fig. 5.** Transition patterns in terms of cortical hierarchy. (A) Hierarchical cortical organization according to a model of the cortical hierarchy developed in non-human primates (Mesulam, 1998). (B) fMPA patterns weighted according to mean hierarchical levels. Red bars indicate the point that exhibited maximum fMPA value. (C) Connectome topology analysis according to hierarchical levels. Proportion of rich-club nodes, connectivity distance, and network communication ratio are reported with respect to the different levels of cortical hierarchy. (D) Correlation between sG1 and  $\Delta fMPA$ , and mean hierarchical level for every pair of state transitions. The magnitude of structure-function coupling is quantified according to the mean hierarchical levels on the right side, showing highest coupling in low hierarchical levels and lowest in high levels.

2017; Margulies et al., 2016; Paquola et al., 2019; Shine et al., 2019; Vos de Wael et al., 2020), they remained underexplored in the analysis of dMRI-derived connectomes. Conceptual work has advocated for the use of gradients to capture subregional heterogeneity and multiplicity (Haak and Beckmann, 2020; Margulies et al., 2016), yet, only few applications leveraged manifold learning on dMRI tractography data and these were mainly restricted to individual regions (Beckmann et al., 2009; Cerlani et al., 2012) or specific lobes (Bajada et al., 2017), often to guide subregional parcellations. In contrast, directly analyzing the low dimensional spaces obtained from dMRI data revealed that these gradients can serve as a powerful coordinate system to visualize and contextualize functional dynamics at macroscale. Similar to classical sensory-transmodal gradients derived from myelin sensitive MRI, as well as resting-state functional connectivity data (Hong et al., 2019; Larivière et al., 2019a; Margulies et al., 2016; Paquola et al., 2019), dMRI gradients are anchored by sensory and motor systems, and guided by spatial proximity. On the other hand, dMRI manifolds ap-

peared less specific to the transmodal and paralimbic system than rs-fMRI and myelin sensitive measures, both of which capture spatially distributed, potentially polysynaptic cortical systems, such as the default mode or frontoparietal network (Hong et al., 2019; Larivière et al., 2019a; Margulies et al., 2016; Paquola et al., 2019). Our study shows that the application of gradient methods to dMRI metrics can complement graph theoretical analyses, suggesting that including both approaches in future approaches could help refine our understanding of structure-function relationships more generally.

Having delineated the principal dimensions of cortical structural connectivity, we used these to interrogate the capacity of this manifold to describe structure-function coupling. An increasing body of prior work studied the correspondence between brain structure and function, using statistical analyses (Messelé et al., 2014; Mišić et al., 2016), communication models (Goñi et al., 2014; Mišić et al., 2015), biophysical simulations (Breakspear, 2017; Deco et al., 2009; Honey et al., 2009; Wang et al., 2019), and artificial intelligence (Rosenthal et al., 2018).

Here, we expanded from prior work assuming stationarity in brain function by inferring time-varying functional states and their transitions (Gotts et al., 2020; Hansen et al., 2015; Vidaurre et al., 2018, 2017) using HMMs to describe dynamic neural changes that emerge during wakeful rest. Our analysis highlighted a temporal hierarchy that reflects a division between low-level sensorimotor and higher-order transmodal states, replicating earlier applications of HMMs to resting-state data (Vidaurre et al., 2017). Importantly, relating these distinct functional states to structural connectome manifolds, we found that they were uniquely related to complementary features of cortical organization. Structural connectome dimensions were particularly useful in describing transitions between low-level functional states and between low- and high-level states. On the other hand, they could not strongly capture transitions within the transmodal regime, a pattern that echoes prior findings that close relationships between structure and function exist in primary sensorimotor areas while the associations become increasingly divergent in transmodal cortices (Park and Friston, 2013; Vázquez-Rodríguez et al., 2019). Notably, structure-function coupling was more marked for the first structural gradient, while the second gradient did not reveal a significant association with function. However, when we incorporated both gradients into a common linear regression, the second gradient indeed improved model performance. A potential explanation for these increases is the interaction between the first two gradients, which might come from continuously changing connectivity patterns as well as potentially overlapping multiple gradients (Haak et al., 2018; Haak and Beckmann, 2020). Topological parameterization based on connectivity distance and rich-club taxonomy related the dynamic functional findings to two important features of core-periphery distinction established by graph theoretical studies (de Reus and van den Heuvel, 2013; Griffa and van den Heuvel, 2018; Liang et al., 2018; Shu et al., 2018; van den Heuvel et al., 2012; Zhao et al., 2017). In fact, dynamic transitions in the sensorimotor state-space engaged mainly short- and intermediary-range connections, while transitions within the higher-order meta-state increasingly occupied rich-club nodes that are mutually interconnected by long-range connections. The differential occupation of nodes with a more regional versus a more large-scale connectivity pattern in lower versus higher-order functional states may reflect different ways they relate to large-scale brain dynamics, with nodes involved in more segregated sensorimotor states having a more localized connectivity profile while higher-order functions are orchestrated by nodes with a more integrated connectivity profile. This conclusion is consistent with our application of connectome-informed communication models, which assume functional signal transmission occurs along structural network edges (Avena-Koenigsberger et al., 2019, 2018; Goñi et al., 2014). We established that sensorimotor states and their transitions frequently involve decentralized mechanisms of network diffusion, where signals diffuse locally without necessarily traversing along the shortest possible paths. In contrast, functional transitions within the transmodal regime increasingly leverage centralized, and globally efficient, routing strategies to maintain long-range communication across distributed hubs. These results, therefore, highlight that dynamic information flow in the brain adheres to different modes of communication, ranging from more decentralized network diffusion processes that run within multiple parallel hierarchies anchored on specific sensorimotor systems towards connector nodes on the one hand, and a more centralized and topology-sensitive routing mechanism that enables the brain-wide integration of the information aggregated by these hubs in a globally efficient manner, on the other (Avena-Koenigsberger et al., 2019, 2018, 2014; Goñi et al., 2014). Future work may determine whether these different communication processes are mediated by different signaling properties. A prior computational model of non-human primate cortical dynamics that incorporated a gradient of synaptic excitation suggested multiple temporal hierarchies across the cortex, with lower-level sensorimotor areas involving fast signaling mechanisms while higher-order cognitive areas demonstrated slow and integrated activity (Chaudhuri et al., 2015). In that study, hierarchical position was

found to correlate with the number of synaptic spines representing a plausible microcircuit substrate underlying an area's capacity to engage in integrative function. The current study adopted mean first-passage time and path length, as well as search information and path transitivity, to explore structurally-governed network communication mechanisms underlying dynamic functional states. These metrics represent a spectrum of communication processes anchored on shortest path communication (*i.e.*, routing) at one extreme, and random walk processes (*i.e.*, diffusion) at the other extreme (Avena-Koenigsberger et al., 2019, 2018). Communication models residing between these two extremes may include (i) communicability, which considers non-shortest paths to characterize complex networks (Estrada and Hatano, 2008), (ii) navigation, a decentralized network communication strategy that captures long and inefficient paths as well as shortest paths (Seguin et al., 2019, 2018), and (iii) spreading models, which describe how local perturbations trigger global cascades (Mišić et al., 2015). These communication models may provide additional information for understanding the correspondence of brain structure and function (Baum et al., 2020; Hermundstad et al., 2013; Honey et al., 2009; Mišić et al., 2016; Osmanlıoğlu et al., 2019; Seguin et al., 2020; Snyder and Bauer, 2019; Suárez et al., 2020; Vázquez-Rodríguez et al., 2019) beyond our current findings based on diffusion and routing. An interesting future direction to link brain structure and functional dynamics may capitalize on asymmetric communication measures (Avena-Koenigsberger et al., 2019, 2018; Goñi et al., 2014, 2013; Rubinov and Sporns, 2010). A recent study estimated send-receive communication asymmetry from undirected structural connectome data, and found that this asymmetry recapitulated functional gradients differentiating low-level sensory to higher-order transmodal areas (Seguin et al., 2019). It may be of interest to explore whether the asymmetric measures can further be associated to communication mechanisms across different structurally-determined and temporal hierarchies, particularly in transmodal networks and a higher-order dynamic state space.

Our findings were consistent across different HCP subsamples and could be replicated in an independent dataset. We also assessed the consistency of our findings across different spatial scales. Findings were consistent at parcellations with 200 and 300 parcels. We found fairly consistent structure-function coupling, where transitions within sensorimotor state and between the meta-states showed high correlations. Unlike the main findings based on 200 parcels, brain regions from 400 node parcellation showed non-significant correlation between sG1 and transitions from fM1 to fM2, and significant correlation with transitions within fM2. This discrepancy may be due to the parcellation approach, which may potentially mix the fMRI signals from different set of vertices. However, why the association between structural manifolds and functional dynamics vary across different parcellation scales needs to be investigated further.

Finally, we also re-expressed our main findings by leveraging a well-established model of cortical hierarchical organization developed in non-human primates (Mesulam, 1998). This model-based analysis confirmed that rich-club proportion, overall connectivity distance, and the increasing use of network routing relative to diffusion increases along the putative cortical hierarchy. Similarly, this analysis also established how the coupling between structure and dynamic functional transitions related to hierarchical levels. Local structural constraints on functional dynamics may be particularly strong when state transitions involve low-level cortical systems and when transitions involve bottom-up and top-down changes in hierarchical levels, but they may not have such a tight grip on transitions occurring within the higher-order regime of cortical hierarchy. Contemporary perspectives on brain wide information processing often focus on the process through which sensorimotor inputs gain access to a global workspace that allows these information to be processed in an explicit conscious manner (Dehaene et al., 1998; Mashour et al., 2020). It is possible that neural dynamics within higher hierarchical levels increasingly engage polysynaptic mechanisms that allow for integrated and flexible processing, which ultimately allows for

the implementation of adaptive control processes for which conscious experience is argued to be important (Mesulam, 1990).

In sum, our study provides a novel perspective on one of the major questions in systems neuroscience: How does the hard-wired structure of the cortex support dynamic functional changes that are necessary for flexible cognition? Our results suggest that this is achieved by balancing local and distant influences in structural constraints. We established that dynamic modes of neural function that are closely linked to lower-level sensorimotor systems are constrained by local features of cortex. In contrast, neural function linked to transmodal regions emerge within a set of constraints that reflect the long-range network routing. Our study, thus, suggests that the wiring of the human brain implements local and distal communication strategies, and that the balance of these two aspects of the structural connectome may be important in supporting both specialized and integrated aspects of cognitive processing.

## Declaration of Competing Interest

The authors declare no conflicts of interest.

## Acknowledgements

Dr. Bo-yong Park was funded by the National Research Foundation of Korea (NRF-2020R1A6A3A03037088), Molson Neuro-Engineering fellowship by Montreal Neurological Institute and Hospital (MNI) and a postdoctoral fellowship of the Fonds de la Recherche du Quebec – Santé (FRQ-S). Mr. Reinder Vos de Wael was funded by a studentship of the Savoy Foundation. Dr. Casey Paquola was funded through a postdoctoral fellowship of the FRQ-S. Ms. Sara Larivière was funded by the Canadian Institutes of Health Research (CIHR). Dr. Oualid Benkarim was funded by a Healthy Brains for Healthy Lives (HBHL) postdoctoral fellowship. Dr. Jessica Royer was supported by a Canadian Open Neuroscience Platform (CONP) fellowship and CIHR. Dr. Raul R. Cruces was funded through a postdoctoral fellowship of the FRQ-S. Dr. Danilo Bzdok was supported by the Healthy Brains Healthy Lives initiative (Canada First Research Excellence fund), and by the CIFAR Artificial Intelligence Chairs program (Canada Institute for Advanced Research). Dr. Jonathan Smallwood was supported by the European Research Council (WANDERINGMINDS-ERC646927). Dr. Boris Bernhardt acknowledges research support from the National Science and Engineering Research Council of Canada (NSERC Discovery-1304413), the Canadian Institutes of Health Research (CIHR FDN-154298), SickKids Foundation (NI17-039), Azrieli Center for Autism Research (ACAR-TACC), BrainCanada, FRQ-S and the Tier-2 Canada Research Chairs program. Data were provided, in part, by the Human Connectome Project, WU-Minn Consortium (Principal Investigators: David Van Essen and Kamil Ugurbil; 1U54MH091657) funded by the 16 NIH Institutes and Centers that support the NIH Blueprint for Neuroscience Research; and by the McDonnell Center for Systems Neuroscience at Washington University. Drs. Bo-yong Park, Casey Paquola, and Boris C. Bernhardt are jointly funded through an MNI-Cambridge collaborative award.

## Data and code availability

The full imaging and phenotypic data from the Human Connectome Project are provide (<https://www.humanconnectome.org/>). MICA-MTL data will be made available via osf.io upon publication of the paper. The codes are available at <https://github.com/MICA-MNI/BrainSpace> (for manifold identification), <https://github.com/OHBA-analysis/HMM-MAR> (for dynamic connectivity analysis), and <https://sites.google.com/site/bctnet/> (for calculating connectome topology).

## Supplementary materials

Supplementary material associated with this article can be found, in the online version, at doi:[10.1016/j.neuroimage.2020.117429](https://doi.org/10.1016/j.neuroimage.2020.117429).

## References

- Alexander-Bloch, A.F., Shou, H., Liu, S., Satterthwaite, T.D., Glahn, D.C., Shinohara, R.T., Vandekar, S.N., Raznahan, A., 2018. On testing for spatial correspondence between maps of human brain structure and function. *Neuroimage* 178, 540–551. doi:[10.1016/j.neuroimage.2018.05.070](https://doi.org/10.1016/j.neuroimage.2018.05.070).
- Allen, E.A., Damaraju, E., Plis, S.M., Erhardt, E.B., Eichele, T., Calhoun, V.D., 2012. Tracking whole-brain connectivity dynamics in the resting state. *Cereb. Cortex* 24, 663–676. doi:[10.1093/cercor/bhs352](https://doi.org/10.1093/cercor/bhs352).
- Ashourvan, A., Gu, S., Mattar, M.G., Vettel, J.M., Bassett, D.S., 2017. The energy landscape underpinning module dynamics in the human brain connectome. *Neuroimage* 157, 364–380. doi:[10.1016/j.neuroimage.2017.05.067](https://doi.org/10.1016/j.neuroimage.2017.05.067).
- Avena-Koenigsberger, A., Goñi, J., Betzel, R.F., van den Heuvel, M.P., Griffa, A., Hagmann, P., Thiran, J.P., Sporns, O., 2014. Using Pareto optimality to explore the topology and dynamics of the human connectome. *Philos. Trans. R. Soc. B Biol. Sci.* 369, doi:[10.1098/rstb.2013.0530](https://doi.org/10.1098/rstb.2013.0530).
- Avena-Koenigsberger, A., Misic, B., Sporns, O., 2018. Communication dynamics in complex brain networks. *Nat. Rev. Neurosci.* 19, 17–33. doi:[10.1038/nrn.2017.149](https://doi.org/10.1038/nrn.2017.149).
- Avena-Koenigsberger, A., Yan, X., Kolchinsky, A., van den Heuvel, M.P., Hagmann, P., Sporns, O., 2019. A spectrum of routing strategies for brain networks. *PLoS Comput. Biol.* 15, 1–24. doi:[10.1371/journal.pcbi.1006833](https://doi.org/10.1371/journal.pcbi.1006833).
- Bajada, C.J., Jackson, R.L., Haroon, H.A., Azadbakht, H., Parker, G.J.M., Ralph, Lambon, M.A., Cloutman, 2017. A graded tractographic parcellation of the temporal lobe. *Neuroimage* 155, 503–512. doi:[10.1016/j.neuroimage.2017.04.016](https://doi.org/10.1016/j.neuroimage.2017.04.016).
- Bassett, D.S., Wymbs, N.F., Porter, M.A., Mucha, P.J., Carlson, J.M., Grafton, S.T., 2011. Dynamic reconfiguration of human brain networks during learning. *Proc. Natl. Acad. Sci. U. S. A.* 108, 7641–7646. doi:[10.1073/pnas.1018985108](https://doi.org/10.1073/pnas.1018985108).
- Batista-García-Ramó, K., Fernández-Verdecia, C.I., 2018. What we know about the brain structure-function relationship. *Behav. Sci. (Basel)* 8, 39. doi:[10.3390-bs8040039](https://doi.org/10.3390-bs8040039).
- Baum, G.L., Cui, Z., Roalf, D.R., Ciric, R., Betzel, R.F., Larsen, B., Cieslak, M., Cook, P.A., Xia, C.H., Moore, T.M., Ruparel, K., Oathes, D.J., Alexander-Bloch, A.F., Shinohara, R.T., Raznahan, A., Gur, R.E., Gur, R.C., Bassett, D.S., Satterthwaite, T.D., 2020. Development of structure-function coupling in human brain networks during youth. *Proc. Natl. Acad. Sci. U. S. A.* 117, 771–778. doi:[10.1073/pnas.1912034117](https://doi.org/10.1073/pnas.1912034117).
- Becker, C.O., Pequito, S., Pappas, G.J., Miller, M.B., Grafton, S.T., Bassett, D.S., Preciado, V.M., 2018. Spectral mapping of brain functional connectivity from diffusion imaging. *Sci. Rep.* 8, 1411. doi:[10.1038/s41598-017-18769-x](https://doi.org/10.1038/s41598-017-18769-x).
- Beckmann, M., Johansen-Berg, H., Rushworth, M.F.S., 2009. Connectivity-based parcellation of human cingulate cortex and its relation to functional specialization. *J. Neurosci.* 29, 1175–1190. doi:[10.1523/JNEUROSCI.3328-08.2009](https://doi.org/10.1523/JNEUROSCI.3328-08.2009).
- Benjamini, Y., Hochberg, Y., 1995. Controlling the false discovery rate : a practical and powerful approach to multiple testing. *J. R. Stat. Soc. Ser. B Stat. Methodol.* 57, 289–300.
- Bertolero, M.A., Yeo, Thomas, B.T., D'Esposito, 2015. The modular and integrative functional architecture of the human brain. *Proc. Natl. Acad. Sci. U. S. A.* 112, E6798–E6807. doi:[10.1073/pnas.1510619112](https://doi.org/10.1073/pnas.1510619112).
- Betzel, R.F., Griffa, A., Hagmann, P., Mišić, B., 2019. Distance-dependent consensus thresholds for generating group-representative structural brain networks. *Netw. Neurosci.* 3, 475–496. doi:[10.1162/netw\\_a\\_00075](https://doi.org/10.1162/netw_a_00075).
- Blondel, V.D., Guillaume, J.L., Lambiotte, R., Lefebvre, E., 2008. Fast unfolding of communities in large networks. *J. Stat. Mech. Theory Exp.* 2008, doi:[10.1088/1742-5468/2008/10/P10008](https://doi.org/10.1088/1742-5468/2008/10/P10008).
- Braun, U., Schäfer, A., Walter, H., Erk, S., Romanczuk-Seifert, N., Haddad, L., Schweiger, J.I., Grimm, O., Heinze, A., Tost, H., Meyer-Lindenberg, A., Bassett, D.S., 2015. Dynamic reconfiguration of frontal brain networks during executive cognition in humans. *Proc. Natl. Acad. Sci. U. S. A.* 112, 11678–11683. doi:[10.1073/pnas.1422487112](https://doi.org/10.1073/pnas.1422487112).
- Breakspear, M., 2017. Dynamic models of large-scale brain activity. *Nat. Neurosci.* 20, 340–352. doi:[10.1038/nn.4497](https://doi.org/10.1038/nn.4497).
- Bullmore, E., Sporns, O., 2009. Complex brain networks: graph theoretical analysis of structural and functional systems. *Nat. Neurosci.* 10, 186–198. doi:[10.1038/nrn2575](https://doi.org/10.1038/nrn2575).
- Burt, J.B., Demirtaş, M., Eckner, W.J., Navejar, N.M., Ji, J.L., Martin, W.J., Bernacchia, A., Anticevic, A., Murray, J.D., 2018. Hierarchy of transcriptomic specialization across human cortex captured by structural neuroimaging topography. *Nat. Neurosci.* 21, 1251–1259. doi:[10.1038/s41593-018-0195-0](https://doi.org/10.1038/s41593-018-0195-0).
- Cerliani, L., Thomas, R.M., Jbabdi, S., Siero, J.C.W., Nanetti, L., Crippa, A., Gazzola, V., D'Arceuil, H., Keyser, C., 2012. Probabilistic tractography recovers a rostral-caudal trajectory of connectivity variability in the human insular cortex. *Hum. Brain Mapp.* 33, 2005–2034. doi:[10.1002/hbm.21338](https://doi.org/10.1002/hbm.21338).
- Chai, L.R., Khambhati, A.N., Ciric, R., Moore, T.M., Gur, R.C., Gur, R.E., Satterthwaite, T.D., Bassett, D.S., 2017. Evolution of brain network dynamics in neurodevelopment. *Netw. Neurosci.* 1, 14–30. doi:[10.1162/netw\\_a\\_00001](https://doi.org/10.1162/netw_a_00001).
- Chai, L.R., Mattar, M.G., Blank, I.A., Fedorenko, E., Bassett, D.S., 2016. Functional network dynamics of the language system. *Cereb. Cortex* 26, 4148–4159. doi:[10.1093/cercor/bhw238](https://doi.org/10.1093/cercor/bhw238).
- Chaudhuri, R., Knoblauch, K., Gariel, M.A., Kennedy, H., Wang, X.J., 2015. A large-scale circuit mechanism for hierarchical dynamical processing in the primate cortex. *Neuron* 88, 419–431. doi:[10.1016/j.neuron.2015.09.008](https://doi.org/10.1016/j.neuron.2015.09.008).
- Christiaens, D., Reisert, M., Dhollander, T., Sunaert, S., Suetens, P., Maes, F., 2015. Global tractography of multi-shell diffusion-weighted imaging data using a multi-tissue model. *Neuroimage* 123, 89–101. doi:[10.1016/j.neuroimage.2015.08.008](https://doi.org/10.1016/j.neuroimage.2015.08.008).
- Ciric, R., Nomi, J.S., Uddin, L.Q., Satpute, A.B., 2017. Contextual connectivity: A framework for understanding the intrinsic dynamic architecture of large-scale functional brain networks. *Sci. Rep.* 7, 6537. doi:[10.1038/s41598-017-06866-w](https://doi.org/10.1038/s41598-017-06866-w).
- Cox, R.W., 1996. AFNI : software for analysis and visualization of functional magnetic resonance neuroimages. *Comput. Biomed. Res.* 29, 162–173. doi:[10.1006/cbmr.1996.0014](https://doi.org/10.1006/cbmr.1996.0014).

- Dale, A.M., Fischl, B., Sereno, M.I., 1999. Cortical surface-based analysis: I. Segmentation and surface reconstruction. *Neuroimage* 9, 179–194. doi:[10.1006/nimg.1998.0395](https://doi.org/10.1006/nimg.1998.0395).
- Damaraju, E., Allen, E.A., Belger, A., Ford, J.M., McEwen, S., Mathalon, D.H., Mueller, B.A., Pearson, G.D., Potkin, S.G., Preda, A., Turner, J.A., Vaidya, J.G., Van Erp, T.G., Calhoun, V.D., 2014. Dynamic functional connectivity analysis reveals transient states of dysconnectivity in schizophrenia. *NeuroImage Clin.* 5, 298–308. doi:[10.1016/j.nicl.2014.07.003](https://doi.org/10.1016/j.nicl.2014.07.003).
- de Reus, M.A., van den Heuvel, M.P., 2013. Rich club organization and intermodule communication in the cat connectome. *J. Neurosci.* 33, 12929–12939. doi:[10.1523/jneurosci.1448-13.2013](https://doi.org/10.1523/jneurosci.1448-13.2013).
- Deco, G., Jirs, V., McIntosh, A.R., Sporns, O., Kotter, R., 2009. Key role of coupling, delay, and noise in resting brain fluctuations. *Proc. Natl. Acad. Sci. U. S. A.* 106, 10302–10307. doi:[10.1073/pnas.0901831106](https://doi.org/10.1073/pnas.0901831106).
- Dehaene, S., Kerszberg, M., Changeux, J.P., 1998. A neuronal model of a global workspace in effortful cognitive tasks. *Proc. Natl. Acad. Sci. U. S. A.* 95, 14529–14534. doi:[10.1073/pnas.95.24.14529](https://doi.org/10.1073/pnas.95.24.14529).
- Ecker, C., Ronan, L., Feng, Y., Daly, E., Murphy, C., Ginestet, C.E., Brammer, M., Fletcher, P.C., Bullmore, E.T., Suckling, J., Baron-Cohen, S., Williams, S., Loth, E., Murphy, D.G.M., 2013. Intrinsic gray-matter connectivity of the brain in adults with autism spectrum disorder. *Proc. Natl. Acad. Sci. U. S. A.* 110, 13222–13227. doi:[10.1073/pnas.1221880110](https://doi.org/10.1073/pnas.1221880110).
- Estrada, E., Hatano, N., 2008. Communicability in complex networks. *Phys. Rev. E - Stat. Nonlinear, Soft Matter Phys.* 77, 1–12. doi:[10.1103/PhysRevE.77.036111](https://doi.org/10.1103/PhysRevE.77.036111).
- Fischl, B., 2012. FreeSurfer. *Neuroimage* 62, 774–781. doi:[10.1016/j.neuroimage.2012.01.021](https://doi.org/10.1016/j.neuroimage.2012.01.021).
- Fischl, B., Sereno, M.I., Dale, A.M., 1999a. Cortical surface-based analysis: II. Inflation, flattening, and a surface-based coordinate system. *Neuroimage* 9, 195–207. doi:[10.1006/nimg.1998.0396](https://doi.org/10.1006/nimg.1998.0396).
- Fischl, B., Sereno, M.I., Tootell, R.B.H., Dale, A.M., 1999b. High-resolution inter-subject averaging and a surface-based coordinate system. *Hum. Brain Mapp.* 8, 272–284. doi:[10.1002/\(SICI\)1097-0193\(1999\)8:3<272::AID-HBM1>3.0.CO;2-1](https://doi.org/10.1002/(SICI)1097-0193(1999)8:3<272::AID-HBM1>3.0.CO;2-1).
- Fornito, A., Zalesky, A., Bullmore, E., 2016. *Fundamentals of Brain Network Analysis*. Academic Press, Amsterdam.
- Friston, K.J., Harrison, L., Penny, W., 2003. Dynamic causal modelling. *Neuroimage* 19, 1273–1302. doi:[10.1016/S1053-8119\(03\)00202-7](https://doi.org/10.1016/S1053-8119(03)00202-7).
- Glasser, M.F., Coalson, T.S., Robinson, E.C., Hacker, C.D., Harwell, J., Yacoub, E., Ugurbil, K., Andersson, J., Beckmann, C.F., Jenkinson, M., Smith, S.M., Van Essen, D.C., 2016. A multi-modal parcellation of human cerebral cortex. *Nature* 536, 171–178. doi:[10.1038/nature18933](https://doi.org/10.1038/nature18933).
- Glasser, M.F., Sotiropoulos, S.N., Wilson, J.A., Coalson, T.S., Fischl, B., Andersson, J.L., Xu, J., Jbabdi, S., Webster, M., Polimeni, J.R., Van Essen, D.C., Jenkinson, M., 2013. The minimal preprocessing pipelines for the human connectome project. *Neuroimage* 80, 105–124. doi:[10.1016/j.neuroimage.2013.04.127](https://doi.org/10.1016/j.neuroimage.2013.04.127).
- Goñi, J., Avena-Koenigsberger, A., Velez de Mendizabal, N., van den Heuvel, M.P., Betzel, R.F., Sporns, O., 2013. Exploring the morphospace of communication efficiency in complex networks. *PLoS One* 8. doi:[10.1371/journal.pone.0058070](https://doi.org/10.1371/journal.pone.0058070).
- Goñi, J., van den Heuvel, M.P., Avena-Koenigsberger, A., De Mendizabal, N.V., Betzel, R.F., Griffa, A., Hagmann, P., Corominas-Murtra, B., Thiran, J.P., Sporns, O., 2014. Resting-brain functional connectivity predicted by analytic measures of network communication. *Proc. Natl. Acad. Sci. U. S. A.* 111, 833–838. doi:[10.1073/pnas.1315529111](https://doi.org/10.1073/pnas.1315529111).
- Gotts, S.J., Gilmore, A.W., Martin, A., 2020. Brain networks, dimensionality, and global signal averaging in resting-state fMRI: Hierarchical network structure results in low-dimensional spatiotemporal dynamics. *Neuroimage* 205, 116289. doi:[10.1016/j.neuroimage.2019.116289](https://doi.org/10.1016/j.neuroimage.2019.116289).
- Griffa, A., van den Heuvel, M.P., 2018. Rich-club neurocircuitry: Function, evolution, and vulnerability. *Dialogues Clin. Neurosci.* 20, 121–132.
- Haak, K.V., Beckmann, C.F., 2020. Understanding brain organisation in the face of functional heterogeneity and functional multiplicity. *Neuroimage* 220, 117061. doi:[10.1016/j.neuroimage.2020.117061](https://doi.org/10.1016/j.neuroimage.2020.117061).
- Haak, K.V., Marquand, A.F., Beckmann, C.F., 2018. Connectopic mapping with resting-state fMRI. *NeuroImage* 170, 83–94. doi:[10.1016/j.neuroimage.2017.06.075](https://doi.org/10.1016/j.neuroimage.2017.06.075).
- Han, X., Qian, X., Bernstein, J.G., Zhou, H.hui, Franzesi, G.T., Stern, P., Bronson, R.T., Graybiel, A.M., Desimone, R., Boyden, E.S., 2009. Millisecond-timescale optical control of neural dynamics in the nonhuman primate brain. *Neuron* 62, 191–198. doi:[10.1016/j.neuron.2009.03.011](https://doi.org/10.1016/j.neuron.2009.03.011).
- Hansen, E.C.A., Battaglia, D., Spiegler, A., Deco, G., Jirsa, V.K., 2015. Functional connectivity dynamics: modeling the switching behavior of the resting state. *Neuroimage* 105, 525–535. doi:[10.1016/j.neuroimage.2014.11.001](https://doi.org/10.1016/j.neuroimage.2014.11.001).
- Hermundstad, A.M., Bassett, D.S., Brown, K.S., Aminoff, E.M., Clewett, D., Freeman, S., Fritsch, A., Johnson, A., Tipper, C.M., Miller, M.B., Grafton, S.T., Carlson, J.M., 2013. Structural foundations of resting-state and task-based functional connectivity in the human brain. *Proc. Natl. Acad. Sci. U. S. A.* 110, 6169–6174. doi:[10.1073/pnas.1219562110](https://doi.org/10.1073/pnas.1219562110).
- Honey, C.J., Sporns, O., Cammoun, L., Gigandet, X., Thiran, J.P., Meuli, R., Hagmann, P., 2009. Predicting human resting-state functional connectivity from structural connectivity. *Proc. Natl. Acad. Sci. U. S. A.* 106, 2035–2040. doi:[10.1073/pnas.0811168106](https://doi.org/10.1073/pnas.0811168106).
- Hong, S.J., Valk, S.L., Di Martino, A., Milham, M.P., Bernhardt, B.C., 2018. Multidimensional neuroanatomical subtyping of autism spectrum disorder. *Cereb. Cortex* 28, 3578–3588. doi:[10.1093/cercor/bhx229](https://doi.org/10.1093/cercor/bhx229).
- Hong, S.-J., Vos De Wael, R., Bethlehem, R.A.I., Lariviere, S., Paquola, C., Valk, S.L., Milham, M.P., Martino, A.Di, Margulies, D.S., Smallwood, J., Bernhardt, B.C., 2019. Atypical functional connectome hierarchy in autism. *Nat. Commun.* 10, 1022.
- Huntenburg, J.M., Bazin, P.L., Goulas, A., Tardif, C.L., Villringer, A., Margulies, D.S., 2017. A systematic relationship between functional connectivity and intracortical myelin in the human cerebral cortex. *Cereb. cortex* 27, 981–997. doi:[10.1093/cercor/bhw030](https://doi.org/10.1093/cercor/bhw030).
- Huntenburg, J.M., Bazin, P.L., Margulies, D.S., 2018. Large-scale gradients in human cortical organization. *Trends Cogn. Sci.* doi:[10.1016/j.tics.2017.11.002](https://doi.org/10.1016/j.tics.2017.11.002).
- Jenkinson, M., Beckmann, C.F., Behrens, T.E.J., Woolrich, M.W., Smith, S.M., 2012. Fsl. *Neuroimage* 62, 782–790. doi:[10.1016/j.neuroimage.2011.09.015](https://doi.org/10.1016/j.neuroimage.2011.09.015).
- Jeurissen, B., Tournier, J.D., Dhollander, T., Connelly, A., Sijbers, J., 2014. Multi-tissue constrained spherical deconvolution for improved analysis of multi-shell diffusion MRI data. *Neuroimage* 103, 411–426. doi:[10.1016/j.neuroimage.2014.07.061](https://doi.org/10.1016/j.neuroimage.2014.07.061).
- Khambhati, A.N., Davis, K.A., Oommen, B.S., Chen, S.H., Lucas, T.H., Litt, B., Bassett, D.S., 2015. Dynamic network drivers of seizure generation, propagation and termination in human neocortical epilepsy. *PLoS Comput. Biol.* 11, 1–19. doi:[10.1371/journal.pcbi.1004608](https://doi.org/10.1371/journal.pcbi.1004608).
- Khambhati, A.N., Sizemore, A.E., Betzel, R.F., Bassett, D.S., 2018. Modeling and interpreting mesoscale network dynamics. *Neuroimage* 180, 337–349. doi:[10.1016/j.neuroimage.2017.06.029](https://doi.org/10.1016/j.neuroimage.2017.06.029).
- Kodinariya, T.M., Makwana, P.R., 2013. Review on determining number of cluster in K-Mean clustering. *Int. J. Adv. Res. Comput. Sci. Manag. Stud.* 1, 90–95.
- Kriegeskorte, N., Simmons, W.K., Bellgowan, P.S., Baker, C.I., 2009. Circular analysis in systems neuroscience: the dangers of double dipping. *Nat. Neurosci.* 12, 535–540. doi:[10.1038/nn.2303](https://doi.org/10.1038/nn.2303).
- Kucyi, A., Tambini, A., Sadaghiani, S., Keilholz, S., Cohen, J.R., 2018. Spontaneous cognitive processes and the behavioral validation of time-varying brain connectivity. *Netw. Neurosci.* 2, 397–417. doi:[10.1162/netn\\_a00037](https://doi.org/10.1162/netn_a00037).
- Lariviére, S., Vos de Wael, R., Hong, S.-J., Paquola, C., Tavakol, S., Lowe, A.J., Schrader, D.V., Bernhardt, B.C., 2019a. Multiscale structure-function gradients in the neonatal connectome. *Cereb. Cortex* doi:[10.1093/cercor/bhz069](https://doi.org/10.1093/cercor/bhz069).
- Lariviére, S., Weng, Y., Wan, R.V., de Frauscher, B., Wang, Z., Bernasconi, A., Bernasconi, N., Schrader, D. V., Zhang, Z., Bernhardt, B.C., 2019b. Functional connectome contractions in temporal lobe epilepsy. *bioRxiv* 756494. doi:[10.1101/756494](https://doi.org/10.1101/756494).
- Lee, M.J., Park, B., Cho, S., Park, H., Kim, S.-T., Chung, C.-S., 2019. Dynamic functional connectivity of migraine brain: a resting-state functional magnetic resonance imaging study. *Pain* 160, 2776–2786. doi:[10.1097/j.pain.0000000000001676](https://doi.org/10.1097/j.pain.0000000000001676).
- Liang, X., Hsu, L.M., Lu, H., Sumiyoshi, A., He, Y., Yang, Y., 2018. The rich-club organization in rat functional brain network to balance between communication cost and efficiency. *Cereb. cortex* 28, 924–935. doi:[10.1093/cercor/bhw416](https://doi.org/10.1093/cercor/bhw416).
- Margulies, D.S., Ghosh, S.S., Goulas, A., Falkiewicz, M., Huntenburg, J.M., Langs, G., Bezin, G., Eickhoff, S.B., Castellanos, F.X., Petrides, M., Jefferies, E., Smallwood, J., 2016. Situating the default-mode network along a principal gradient of macroscale cortical organization. *Proc. Natl. Acad. Sci. U. S. A.* 113, 12574–12579. doi:[10.1073/pnas.1608282113](https://doi.org/10.1073/pnas.1608282113).
- Mashour, G.A., Roelfsema, P., Changeux, J.P., Dehaene, S., 2020. Conscious processing and the global neuronal workspace hypothesis. *Neuron* 105, 776–798. doi:[10.1016/j.neuron.2020.01.026](https://doi.org/10.1016/j.neuron.2020.01.026).
- Messé, A., Rudrauf, D., Benali, H., Marrelec, G., 2014. Relating structure and function in the human brain: relative contributions of anatomy, stationary dynamics, and non-stationarities. *PLoS Comput. Biol.* 10, e1003530. doi:[10.1371/journal.pcbi.1003530](https://doi.org/10.1371/journal.pcbi.1003530).
- Mesulam, M.-M., 1990. Large-scale neurocognitive networks and distributed processing for attention, language, and memory. *Ann. Neurol.* 28, 597–613. doi:[10.1002/ana.410280502](https://doi.org/10.1002/ana.410280502).
- Mesulam, M.M., 1998. From sensation to cognition. *Brain* 121, 1013–1052. doi:[10.1093/brain/121.6.1013](https://doi.org/10.1093/brain/121.6.1013).
- Mišić, B., Betzel, R.F., van den Heuvel, M.P., Berman, M.G., McIntosh, A.R., Sporns, O., 2016. Network-level structure-function relationships in human neocortex. *Cereb. Cortex* 26, 3285–3296. doi:[10.1093/cercor/bhw089](https://doi.org/10.1093/cercor/bhw089).
- Mišić, B., Betzel, R.F., Nematzadeh, A., Goñi, J., Griffa, A., Hagmann, P., Flammini, A., Ahn, Y.Y., Sporns, O., 2015. Cooperative and competitive spreading dynamics on the human connectome. *Neuron* 86, 1518–1529. doi:[10.1016/j.neuron.2015.05.035](https://doi.org/10.1016/j.neuron.2015.05.035).
- Oligschläger, S., Xu, T., Baczkowski, B.M., Falkiewicz, M., Falchier, A., Linn, G., Margulies, D.S., 2019. Gradients of connectivity distance in the cerebral cortex of the macaque monkey. *Brain Struct. Funct.* 224, 925–935. doi:[10.1007/s00429-018-1811-1](https://doi.org/10.1007/s00429-018-1811-1).
- Osmانلوğlu, Y., Tunç, B., Parker, D., Elliott, M.A., Baum, G.L., Ciric, R., Satterthwaite, T.D., Gur, R.E., Gur, R.C., Verma, R., 2019. System-level matching of structural and functional connectomes in the human brain. *Neuroimage* 199, 93–104. doi:[10.1016/j.neuroimage.2019.05.064](https://doi.org/10.1016/j.neuroimage.2019.05.064).
- Paquola, C., Vos de Wael, R., Wagstyl, K., Bethlehem, R.A.I., Hong, S.J., Seidlitz, J., Bullmore, E.T., Evans, A.C., Mišić, B., Margulies, D.S., Smallwood, J., Bernhardt, B.C., 2019. Microstructural and functional gradients are increasingly dissociated in transmodal cortices. *PLoS Biol* 17, e3000284. doi:[10.1371/journal.pbio.3000284](https://doi.org/10.1371/journal.pbio.3000284).
- Park, B., Lee, M.J., Kim, M., Kim, S.-H., Park, H., 2018a. Structural and functional brain connectivity changes between people with abdominal and non-abdominal obesity and their association with behaviors of eating disorders. *Front. Neurosci.* 12, 741. doi:[10.3389/fnins.2018.00741](https://doi.org/10.3389/fnins.2018.00741).
- Park, B., Shim, Mok, W., James, O., Park, 2019. Possible links between the lag structure in visual cortex and visual streams using fMRI. *Sci. Rep.* 9, 4283. doi:[10.1038/s41598-019-40728-x](https://doi.org/10.1038/s41598-019-40728-x).
- Park, B., Moon, T., Park, H., 2018b. Dynamic functional connectivity analysis reveals improved association between brain networks and eating behaviors compared to static analysis. *Behav. Brain Res.* 337, 114–121. doi:[10.1016/j.bbr.2017.10.001](https://doi.org/10.1016/j.bbr.2017.10.001).
- Park, H.J., Friston, K., 2013. Structural and functional brain networks: From connections to cognition. *Science* (80-) 342, 1238411. doi:[10.1126/science.1238411](https://doi.org/10.1126/science.1238411).
- Razi, A., Seghier, M.L., Zhou, Y., McColligan, P., Zeidman, P., Park, H., Sporns, O., Rees, G., Friston, K.J., 2017. Large-scale DCMs for resting-state fMRI. *Netw. Neurosci.* 1, 222–241. doi:[10.1162/netn\\_a00037](https://doi.org/10.1162/netn_a00037).

- Robinson, E.C., Jbabdi, S., Glasser, M.F., Andersson, J., Burgess, G.C., Harms, M.P., Smith, S.M., Van Essen, D.C., Jenkinson, M., 2014. MSM: A new flexible framework for Multimodal Surface Matching. *NeuroImage* 100, 414–426. doi:[10.1016/j.neuroimage.2014.05.069](https://doi.org/10.1016/j.neuroimage.2014.05.069).
- Rosenthal, G., Váša, F., Griffa, A., Hagmann, P., Amico, E., Goñi, J., Avidan, G., Sporns, O., 2018. Mapping higher-order relations between brain structure and function with embedded vector representations of connectomes. *Nat. Commun.* 9, 2178. doi:[10.1038/s41467-018-04614-w](https://doi.org/10.1038/s41467-018-04614-w).
- Rubinov, M., Sporns, O., 2010. Complex network measures of brain connectivity: uses and interpretations. *NeuroImage* 52, 1059–1069. doi:[10.1016/j.neuroimage.2009.10.003](https://doi.org/10.1016/j.neuroimage.2009.10.003).
- Rubinov, M., Sporns, O., van Leeuwen, C., Breakspear, M., 2009. Symbiotic relationship between brain structure and dynamics. *BMC Neurosci* 10, 55. doi:[10.1186/1471-2202-10-55](https://doi.org/10.1186/1471-2202-10-55).
- Salimi-Khorshidi, G., Douaud, G., Beckmann, C.F., Glasser, M.F., Griffanti, L., Smith, S.M., 2014. Automatic denoising of functional MRI data: combining independent component analysis and hierarchical fusion of classifiers. *NeuroImage* 90, 449–468. doi:[10.1016/j.neuroimage.2013.11.046](https://doi.org/10.1016/j.neuroimage.2013.11.046).
- Schaefer, A., Kong, R., Gordon, E.M., Laumann, T.O., Zuo, X.-N., Holmes, A.J., Eickhoff, S.B., Yeo, B.T.T., 2018. Local-global parcellation of the human cerebral cortex from intrinsic functional connectivity MRI. *Cereb. Cortex* 28, 3095–3114. doi:[10.1093/cercor/bhx179](https://doi.org/10.1093/cercor/bhx179).
- Seguin, C., Razi, A., Zalesky, A., 2019. Inferring neural signalling directionality from undirected structural connectomes. *Nat. Commun.* 10, 4289. doi:[10.1038/s41467-019-12201-w](https://doi.org/10.1038/s41467-019-12201-w).
- Seguin, C., Tian, Y., Zalesky, A., 2020. Network communication models improve the behavioral and functional predictive utility of the human structural connectome. *Netw. Neurosci* 1–40. doi:[10.1162/netn\\_a\\_00161](https://doi.org/10.1162/netn_a_00161).
- Seguin, C., van den Heuvel, M.P., Zalesky, A., 2018. Navigation of brain networks. *Proc. Natl. Acad. Sci. U. S. A.* 115, 6297–6302. doi:[10.1073/pnas.1801351115](https://doi.org/10.1073/pnas.1801351115).
- Shine, J.M., Breakspear, M., Bell, P.T., Ehgoetz Martens, K., Shine, R., Koyejo, O., Sporns, O., Poldrack, R.A., 2019. Human cognition involves the dynamic integration of neural activity and neuromodulatory systems. *Nat. Neurosci.* 22, 289–296. doi:[10.1038/s41593-018-0312-0](https://doi.org/10.1038/s41593-018-0312-0).
- Shu, N., Duan, Y., Huang, J., Ren, Z., Liu, Z., Dong, H., Barkhof, F., Li, K., Liu, Y., 2018. Progressive brain rich-club network disruption from clinically isolated syndrome towards multiple sclerosis. *NeuroImage Clin.* 19, 232–239. doi:[10.1016/j.niclin.2018.03.034](https://doi.org/10.1016/j.niclin.2018.03.034).
- Smith, R.E., Tournier, J.D., Calamante, F., Connelly, A., 2012. Anatomically-constrained tractography: Improved diffusion MRI streamlines tractography through effective use of anatomical information. *NeuroImage* 62, 1924–1938. doi:[10.1016/j.neuroimage.2012.06.005](https://doi.org/10.1016/j.neuroimage.2012.06.005).
- Smith, R.E., Tournier, J.D., Calamante, F., Connelly, A., 2015. SIFT2: Enabling dense quantitative assessment of brain white matter connectivity using streamlines tractography. *NeuroImage* 119, 338–351. doi:[10.1016/j.neuroimage.2015.06.092](https://doi.org/10.1016/j.neuroimage.2015.06.092).
- Snyder, A.Z., Bauer, A.Q., 2019. Mapping structure-function relationships in the brain. *Biol. Psychiatry Cogn. Neurosci. Neuroimaging* 4, 510–521. doi:[10.1016/j.bpsc.2018.10.005](https://doi.org/10.1016/j.bpsc.2018.10.005).
- Suárez, L.E., Markello, R.D., Betzel, R.F., Misic, B., 2020. Linking structure and function in macroscale brain networks. *Trends Cogn. Sci.* 24, 302–315. doi:[10.1016/j.tics.2020.01.008](https://doi.org/10.1016/j.tics.2020.01.008).
- Taghia, J., Cai, W., Ryali, S., Kochalka, J., Nicholas, J., Chen, T., Menon, V., 2018. Uncovering hidden brain state dynamics that regulate performance and decision-making during cognition. *Nat. Commun.* 9, 2505. doi:[10.1038/s41467-018-04723-6](https://doi.org/10.1038/s41467-018-04723-6).
- Tenenbaum, J.B., Silva, V.de, Langford, J.C., 2000. A global geometric framework for nonlinear dimensionality reduction. *Science* (80-. ) 290, 2319–2323. doi:[10.1126/science.290.5500.2319](https://doi.org/10.1126/science.290.5500.2319).
- Tournier, J.D., Calamante, F., Connelly, A., 2012. MRtrix: diffusion tractography in crossing fiber regions. *Int. J. Imaging Syst. Technol.* 22, 53–66. doi:[10.1002/ima.22005](https://doi.org/10.1002/ima.22005).
- Tournier, J.D., Smith, R., Raffelt, D., Tabbara, R., Dhollander, T., Pietsch, M., Christiaens, D., Jeurissen, B., Yeh, C.H., Connelly, A., 2019. MRtrix3: A fast, flexible and open software framework for medical image processing and visualisation. *NeuroImage* 202, 116137. doi:[10.1016/j.neuroimage.2019.116137](https://doi.org/10.1016/j.neuroimage.2019.116137).
- van den Heuvel, M.P., Kahn, R.S., Goñi, J., Sporns, O., 2012. High-cost, high-capacity backbone for global brain communication. *Proc. Natl. Acad. Sci. U. S. A.* 109, 11372–11377. doi:[10.1073/pnas.1203593109](https://doi.org/10.1073/pnas.1203593109).
- Van Essen, D.C., Glasser, M.F., Dierker, D.L., Harwell, J., Coalson, T., 2012. Parcellations and hemispheric asymmetries of human cerebral cortex analyzed on surface-based atlases. *Cereb. Cortex* 22, 2241–2262. doi:[10.1093/cercor/brz291](https://doi.org/10.1093/cercor/brz291).
- Van Essen, D.C., Smith, S.M., Barch, D.M., Behrens, T.E.J., Yacoub, E., Ugurbil, K., 2013. The WU-Minn human connectome project: an overview. *NeuroImage* 80, 62–79. doi:[10.1016/j.neuroimage.2013.05.041](https://doi.org/10.1016/j.neuroimage.2013.05.041).
- Vázquez-Rodríguez, B., Suárez, L.E., Markello, R.D., Shafiei, G., Paquola, C., Hagmann, P., van den Heuvel, M.P., Bernhardt, B.C., Spreng, R.N., Misic, B., 2019. Gradients of structure-function tethering across neocortex. *Proc. Natl. Acad. Sci. U. S. A.* 116, 21219–21227. doi:[10.1073/pnas.1903403116](https://doi.org/10.1073/pnas.1903403116).
- Vidaurre, D., Abeysuriya, R., Becker, R., Quinn, A.J., Alfaro-Almagro, F., Smith, S.M., Woolrich, M.W., 2018. Discovering dynamic brain networks from big data in rest and task. *NeuroImage* 180, 646–656. doi:[10.1016/j.neuroimage.2017.06.077](https://doi.org/10.1016/j.neuroimage.2017.06.077).
- Vidaurre, D., Quinn, A.J., Baker, A.P., Dupret, D., Tejero-Cantero, A., Woolrich, M.W., 2016. Spectrally resolved fast transient brain states in electrophysiological data. *NeuroImage* 126, 81–95. doi:[10.1016/j.neuroimage.2015.11.047](https://doi.org/10.1016/j.neuroimage.2015.11.047).
- Vidaurre, D., Smith, S.M., Woolrich, M.W., 2017. Brain network dynamics are hierarchically organized in time. *Proc. Natl. Acad. Sci.* 114, 12827–12832. doi:[10.1073/pnas.1705120114](https://doi.org/10.1073/pnas.1705120114).
- Von Luxburg, U., 2007. A tutorial on spectral clustering. *Stat. Comput.* 17, 395–416. doi:[10.1007/s11222-007-9033-z](https://doi.org/10.1007/s11222-007-9033-z).
- Vos de Wael, R., Benkarim, O., Paquola, C., Larivière, S., Royer, J., Tavakol, S., Xu, T., Hong, S.-J., Valk, S.L., Misic, B., Milham, M.P., Margulies, D.S., Smallwood, J., Bernhardt, B.C., 2020. BrainSpace: a toolbox for the analysis of macroscale gradients in neuroimaging and connectomics datasets. *Commun. Biol.* 3, 103. doi:[10.1038/s42003-020-0794-7](https://doi.org/10.1038/s42003-020-0794-7).
- Wang, P., Kong, R., Kong, X., Liégeois, R., Orban, C., Deco, G., van den Heuvel, M.P., Yeo, B.T.T., 2019. Inversion of a large-scale circuit model reveals a cortical hierarchy in the dynamic resting human brain. *Sci. Adv.* 5. doi:[10.1126/sciadv.aat7854](https://doi.org/10.1126/sciadv.aat7854), eaat7854.
- Vos de Wael, R., Larivière, S., Caldairou, B., Hong, S.J., Margulies, D.S., Jefferies, E., Bernasconi, A., Smallwood, J., Bernasconi, N., Bernhardt, B.C., 2018. Anatomical and microstructural determinants of hippocampal subfield functional connectome embedding. *Proc. Natl. Acad. Sci. U. S. A.* 115, 10154–10159. doi:[10.1073/pnas.1803667115](https://doi.org/10.1073/pnas.1803667115).
- Wang, Z., Dai, Z., Gong, G., Zhou, C., He, Y., 2015. Understanding structural-functional relationships in the human brain: A large-scale network perspective. *Neuroscientist* 21, 290–305. doi:[10.1177/1073858414537560](https://doi.org/10.1177/1073858414537560).
- Yarkoni, T., Poldrack, R.A., Nichols, T.E., Van Essen, D.C., Wager, T.D., 2011. Large-scale automated synthesis of human functional neuroimaging data. *Nat. Methods* 8, 665–670. doi:[10.1038/nmeth.1635](https://doi.org/10.1038/nmeth.1635).
- Zhao, X., Tian, L., Yan, J., Yue, W., Yan, H., Zhang, D., 2017. Abnormal Rich-Club Organization Associated with Compromised Cognitive Function in Patients with Schizophrenia and Their Unaffected Parents. *Neurosci. Bull.* 33, 445–454. doi:[10.1007/s12264-017-0151-0](https://doi.org/10.1007/s12264-017-0151-0).